High-dimensional regression with outcomes of mixed-type using the multivariate spike-and-slab LASSO

Soham Ghosh* Sameer K. Deshpande!

June 17, 2025

Abstract

We consider a high-dimensional multi-outcome regression in which q, possibly dependent, binary and continuous outcomes are regressed onto p covariates. We model the observed outcome vector as a partially observed latent realization from a multivariate linear regression model. Our goal is to estimate simultaneously a sparse matrix (B) of latent regression coefficients (i.e., partial covariate effects) and a sparse latent residual precision matrix (Ω) , which induces partial correlations between the observed outcomes. To this end, we specify continuous spike-and-slab priors on all entries of B and off-diagonal elements of Ω and introduce a Monte Carlo Expectation-Conditional Maximization algorithm to compute the maximum a posterior estimate of the model parameters. Under a set of mild assumptions, we derive the posterior contraction rate for our model in the high-dimensional regimes where both p and q diverge with the sample size p and establish a sure screening property, which implies that, as p increases, we can recover all truly non-zero elements of p with probability tending to one. We demonstrate the excellent finite-sample properties of our proposed method, which we call mixed-mSSL, using extensive simulation studies and three applications spanning medicine to ecology.

^{*}Dept. of Statistics, University of Wisconsin-Madison. sghosh39@wisc.edu

[†]Dept. of Statistics, University of Wisconsin-Madison. sameer.deshpande@wisc.edu

1 Introduction

In many applications spanning biology, ecology, and medicine, analysts are interested in understanding the effect of p covariates on q, possibly related outcomes. When all the outcomes are continuous, a multivariate linear regression model is a natural starting point. In this setting, jointly modeling the regression coefficient and residual covariance matrices has many advantages over fitting separate models to each outcome: estimates of the regression coefficients are asymptotically more efficient (Zellner, 1962) and in high-dimensional settings, joint models can detect smaller covariate effects than separate models (Deshpande et al., 2019) and yield improved predictions (Li et al., 2023). But when the outcomes are of mixed-type — that is, when some outcomes are continuous and others are discrete — specifying joint models capturing the residual dependence between the outcomes is much more complicated. While some authors decompose the joint outcomes into a product of conditional densities (see, e.g., Fitzmaurice and Laird, 1997), many others rely on latent variables to induce dependence between discrete and continuous outcomes (see, e.g., Dunson, 2000; McCulloch, 2008; Wagner and Tüchler, 2010; Canale and Dunson, 2011, 2013, 2014; Kowal and Canale, 2020; Bradley, 2022). In this work, we follow these latter examples and express our observed mixed-type outcomes as partially observed realizations from a multivariate linear regression model.

More specifically, suppose that we observe n pairs $(\boldsymbol{x}_1, \boldsymbol{y}_1), \ldots, (\boldsymbol{x}_n, \boldsymbol{y}_n)$ of a p-dimensional covariate vector $\boldsymbol{x} \in \mathbb{R}^p$ and a q-dimensional outcome vector \boldsymbol{y} . To estimate simultaneously the effect of each covariate on each outcome and the residual dependence structure between the outcomes, we introduce a latent variable $\boldsymbol{z} \in \mathbb{R}^q$ such that (i) $\boldsymbol{z} \sim \mathcal{N}_q(\boldsymbol{B}^\top \boldsymbol{x}, \Omega^{-1})$ and (ii) $\boldsymbol{y} = g(\boldsymbol{z})$, where g is a deterministic function (defined formally in Section 2); \boldsymbol{B} is a $p \times q$ matrix of unknown regression coefficients; and Ω is a $q \times q$ positive-definite precision matrix capturing the latent residual dependence structure. Our work is motivated by the following three applications.

- Biomarkers for kidney disease: Ebiaredoh-Mienye et al. (2022) studied the effects of p = 24 clinical covariates on a binary indicator of chronic kidney disease (CKD) status and a continuous measure of urine-specific gravity (SG) using data from n = 400 patients. Here, we wish to identify which clinical covariates are most predictive of both CKD and SG and to quantify the residual dependence between these outcomes unexplained by these covariates.
- Colorectal cancer and the microbiome: Wirbel et al. (2019) conducted a meta-study of five colorectal-cancer (CRC) cohorts totaling n=574 subjects and p=849 prevalent bacterial species in the gut microbiome. While their primary focus was on the binary CRC status, there is growing evidence that both Type-2 diabetes and body-mass index (BMI) share overlapping microbial signatures with CRC risk (Qin et al., 2012; Mandic et al., 2024). In our re-analysis, we wish to identify those specifies most associated with CRC status, diabetes status, and BMI, while simultaneously quantifying their residual dependence.
- Finnish birds: Lindström et al. (2015) surveyed n=137 breeding-season transects in Finland and recorded presence-absence for the q=50 most common bird species, together with four continuous climate covariates. In this context, entries in \boldsymbol{B} capture how changes in climatic conditions affect species' presence while off-diagonal elements in Ω may reflect biotic interactions such as competition or facilitation that cannot be explained by the measured climatic factors alone.

For the motivating CRC and Finnish bird datasets, the total number of model parameters (pq +

q(q-1)/2) exceeds the sample size n. In such high-dimensional settings, it is common to assume that \mathbf{B} and/or Ω is sparse. Shrinkage priors that pull negligible parameter values towards zero while shrinking truly important values less aggressively are extremely popular in the Bayesian literature. Two complementary classes of such priors dominate current practice: (i) global-local shrinkage priors that model parameters as being drawn from continuous scale mixtures (e.g., Bhadra et al., 2017) and (ii) spike-and-slab priors that model parameters as being drawn from either a distribution sharply concentrated at zero (the "spike") or a diffuse distribution (the "slab") (e.g., George and McCulloch, 1993; Ishwaran and Rao, 2005). In mixed-outcome regression, Wang et al. (2025) adopt the first approach: their mt-MBSP model combines a latent-variable construction with horseshoe-type priors to handle $p \gg n$ cases, but it fixes the number of outcomes q and does not learn residual correlations. At the other end, the BS-MRMR framework of Chen et al. (2023) uses spike-and-slab priors with a point-mass spike to estimate both \mathbf{B} and Ω , yet it is feasible only when n > p. Very recent algorithmic advances have begun to scale spike-and-slab learning to high dimensions (Zhou et al., 2022), motivating us to revisit spike-and-slab priors in the mixed-response setting.

Motivated by the simultaneous needs to (i) model both binary and continuous outcomes and (ii) learn a sparse \boldsymbol{B} and a sparse Ω when either p or q grows with n, while remaining computationally feasible, we propose a new method, termed mixed-mSSL. It represents the observed outcomes as a partially observed realization from a multivariate linear regression model with a sparse matrix of covariate effects \boldsymbol{B} and a sparse residual precision matrix Ω . We further specify spike-and-slab LASSO (SSLASSO; Ročková and George, 2018) priors on each element of \boldsymbol{B} and the off-diagonal elements of Ω . In this way, mixed-mSSL generalizes the univariate SSLASSO and its extension to the sparse multivariate linear regression setting (mSSL; Deshpande et al., 2019).

Like these methods, we compute the maximum a posteriori (MAP) estimate of \boldsymbol{B} and Ω using an EM-like algorithm that iteratively solves a series of penalized maximum likelihood problems in which the penalties are adaptively and automatically updated. Because the latent variable \boldsymbol{z} in our model precludes the same type of closed-form E-step calculations underpinning SSLASSO and mSSL, we instead develop a Monte Carlo Expected—Conditional Maximization (MCECM) algorithm. In our algorithm, we iterate between a Monte Carlo E-step, which involves repeatedly sampling the unobserved components of the latent \boldsymbol{z}_i 's from their conditional posterior, and two conditional maximization (CM) steps, in which \boldsymbol{B} and Ω are sequentially updated. In simulation studies, mixed-mSSL demonstrated strong accuracy and specificity for joint variable and covariance selection, outperforming both the Bayesian competitor mt-MBSP and two baseline approaches, one that fits separate spike-and-slab lasso models (sepSSL) to each outcome and another using frequentist elastic-net penalized GLMs (sepglm).

On the motivating CKD data, mixed-mSSL identified several known biomarkers and, unlike competing methods, also flagged random blood glucose as a risk factor — a finding corroborated by other studies. Mixed-mSSL further delivered higher predictive AUC for colorectal cancer (CRC) and diabetes status, as well as lower BMI prediction error, compared to mt-MBSP, sepSSL, and sepglm. On the Finnish bird example, mixed-mSSL uncovered a residual dependence network consistent with known habitat patterns. These empirical results re-iterate the benefits of a joint modeling approach that unifies both continuous and binary responses through latent data augmentation, while directly capturing sparsity in both \boldsymbol{B} and Ω .

From a theoretical standpoint, we derive posterior contraction rates for both B and Ω in the regime

where both the number of covariates p and the number of outcomes q grow with the sample size n. In doing so, our results significantly extend earlier results on posterior consistency for \boldsymbol{B} like Bai and Ghosh (2018), who assumed that q is fixed, and Wang et al. (2025), who did not establish posterior contraction for Ω . Under an additional "beta-min" condition, we further show that mixed-mSSL can consistently recover the non-zero elements of \boldsymbol{B} (Theorem 7).

The rest of the paper is organized as follows. In Section 2, we introduce the mixed-mSSL model in detail before deriving our MCECM algorithm for MAP estimation in Section 3. We state our main theoretical results in Section 4, deferring all proofs to Appendix A. Then, in Section 5, we report the results from several synthetic data simulations comparing mixed-mSSL to several competing methods. We apply mixed-mSSL to each of the three motivating datasets in Section 6 and conclude with a discussion of potential extensions in Section 7. All R codes used to generate the simulation studies and real-data analyses are openly available at the companion GitHub repository https://github.com/ghoshstats/mixed-mSSL.

2 Modeling Mixed-type Responses

Suppose we have n pairs $(\boldsymbol{x}_1, \boldsymbol{y}_1), \dots, (\boldsymbol{x}_n, \boldsymbol{y}_n)$ of covariates $\boldsymbol{x} \in \mathbb{R}^p$ and outcomes $\boldsymbol{y} \in \mathbb{R}^{q_c} \times \{0, 1\}^{q_b}$. We model, for each $i = 1, \dots, n$

$$z_i | \boldsymbol{B}, \Omega \sim \mathcal{N}_q \left(\boldsymbol{B}^{\top} \boldsymbol{x}_i, \Omega^{-1} \right)$$

$$\boldsymbol{y}_i = g(\boldsymbol{z}_i), \tag{1}$$

where the function $q: \mathbb{R}^q \times \mathbb{R}^{q_c} \times \{0,1\}^{q_b}$ operates element-wise and is given by

$$g(z_1, \dots, z_{q_c}, z_{q_c+1}, \dots, z_q) = (z_1, \dots, z_{q_c}, \mathbb{1} (z_{q_c+1} \ge 0), \dots, \mathbb{1} (z_q \ge 0))^{\top}.$$

That is, g leaves the first q_c components of its argument unchanged and thresholds the remaining q_b components at zero. For the latent Gaussian construction in (1), because only the sign of each latent binary coordinate is observed, its scale is not identifiable. We therefore fix the residual variance of every binary latent component to be one; that is, we constrain $\sigma_k^2 := (\Omega^{-1})_{k,k} = 1$ for $k = q_{c+1}, \ldots, q$.

For every covariate-outcome pair (j, k), the entry β_{jk} measures the effect of increasing x_j by one unit while holding the other covariates fixed. For continuous outcomes, $\beta_{j,k}$ is the familiar partial regression coefficient $\beta_{j,k} = \mathbb{E}[Y_k|X_j = x+1, \mathbf{X}_{-j}] - \mathbb{E}[Y_k|X_j = x, \mathbf{X}_{-j}]$, where \mathbf{X}_{-j} is the covariate vector without its j-th entry. For binary outcomes, a first-order Taylor expansion shows that an upper bound of the associated risk difference depends on the magnitude of $\beta_{j,k}$:

$$\mathbb{P}(Y_k = 1 | X_j = x + 1, \boldsymbol{X}_{-j} = \boldsymbol{x}_{-j}) - \mathbb{P}(Y_k = 1 | X_j = x, \boldsymbol{X}_{-j} = \boldsymbol{x}_{-j}) =$$

$$\Phi\left(\beta_{j,k}(x+1) + \sum_{j' \neq j} \beta_{j',k} x_j\right) - \Phi\left(\beta_{j,k} x + \sum_{j' \neq j} \beta_{j',k} x_j\right) \approx$$

$$\beta_{j,k} \phi\left(\left[\beta_{j,k} x + \sum_{j' \neq j} \beta_{j',k} x_j\right]\right) \leq (2\pi)^{-\frac{1}{2}} |\beta_{j,k}|,$$

where ϕ and Φ are the standard normal probability density and cumulative distribution functions.

Our proposed model can be seen as natural generalization of Chib and Greenberg (1998)'s multivariate probit regression model. It is also closely related to the rounding-based approach to modeling count processes developed in Canale and Dunson (2011, 2013, 2014) and later extended by Kowal and Canale (2020). Though we do not pursue it here, by using a slightly different transformation g, our model can easily accommodate count data. Our proposed model is similar to the one studied in Wang et al. (2025), which introduces q_b latent Pólya-Gamma (Polson et al., 2013) variables (one for each binary outcome) that are related to a q-dimensional latent Gaussian z; see Equation 2.6 of Wang et al. (2025) for details. The mmrr model of Ekvall and Molstad (2022) also addresses regression with mixed-type outcomes using latent Gaussian variables. However, their approach fundamentally differs from ours: while our model treats the observed outcomes as deterministic transformations of latent variables (y = g(z)), their method assumes canonical generalized linear model (GLM) links relating the conditional mean of each observed outcome directly to the latent variables (i.e., $\mathbb{E}(Y|Z) = h^{-1}(Z)$ for a known link function h).

The precision matrix Ω in Equation (1) captures residual dependence between the components of the latent variable z. These dependencies in turn induce residual and marginal dependence between the observed outcomes. Although the model allows for arbitrary correlations between elements of the latent z, it limits the range of observable correlations between elements of the observation y.

Lemma 1 (Maximal observed correlation). Consider two response variables Y_k and $Y_{k'}$, for $k \neq k' \in \{1, 2, ..., q\}$, each generated from Equation (1). Then the maximal possible absolute correlation $|\rho_{k,k'}| := |Corr(Y_k, Y_{k'}|\mathbf{X})|$ among the observed outcomes satisfies:

$$|\rho_{k,k'}| \leq \begin{cases} 1, & \text{if both } Y_k, Y_{k'} \text{ are continuous or both are binary,} \\ \sqrt{2/\pi}, & \text{if one of } Y_k, Y_{k'} \text{ is continuous and the other is binary.} \end{cases}$$

In other words, Equation (1) allows for arbitrarily large correlations between two continuous outcomes and two binary outcomes but caps the maximal correlation between a binary and continuous outcome at $\sqrt{2/\pi} \approx 0.798$. In practice, we have not observed this limitation to be much of an issue. The proof in Appendix A.2 follows the same argument of Lemma 2.1 in Ekvall and Molstad (2022) by noting that when Y_k and $Y_{k'}$ are of different type $\operatorname{Corr}(Y_k, Y_{k'}|X) = 2\mathbb{E}[Z_k\mathbb{1}(Z_{k'} > 0)]$ is an integral monotone in $\rho_z = \operatorname{Cor}(Z_k, Z_{k'}|X)$ that, by the Dominated Convergence Theorem, converges to $\sqrt{2/\pi}$ as $\rho_z \to 1$.

2.1 Prior specification

When the total number of parameters in Equation (1), pq+q(q-1)/2, exceeds the sample size, not all the entries in \boldsymbol{B} and Ω are likelihood-identified. To make the estimation problem tractable, it is common to assume that both \boldsymbol{B} and Ω are sparse. Rather than specifying a prior fully supported on exactly sparse matrices, we follow George and McCulloch (1993) and specify continuous spike-and-slab priors on the elements $\beta_{j,k}$ and $\omega_{k,k'}$. In other words, our priors encode the belief that (i) most entries of \boldsymbol{B} and Ω are of essentially negligible magnitude (i.e., they are drawn from the spike) and (ii) only a few entries of much larger magnitude (i.e., they are drawn from the slab). We specifically employ Laplacian spike and slab distributions, which were first introduced in Ročková and George (2018).

Formally, we fix positive constants $0 < \lambda_1 \ll \lambda_0$ and model the entries $\beta_{j,k}$ as being drawn from either a very diffuse Laplace(λ_1) slab or Laplace(λ_0) spike that is sharply concentrated around zero. Letting $\theta \in [0,1]$ be the probability that each $\beta_{j,k}$ is drawn from the slab, our conditional prior density of \boldsymbol{B} is

$$p(\boldsymbol{B}|\theta) = \prod_{j=1}^{p} \prod_{k=1}^{q} \left[\frac{\theta \lambda_1}{2} e^{-\lambda_1 |\beta_{j,k}|} + \frac{(1-\theta)\lambda_0}{2} e^{-\lambda_0 |\beta_{j,k}|} \right].$$

For Ω , it suffices to specify a prior for the diagonal elements $\omega_{k,k}$ and the off-diagonal elements in the upper triangle $\omega_{k,k'}$ with k < k'. To this end, entirely analogously with \mathbf{B} , we fix two more positive constants $0 < \xi_1 \ll \xi_0$; introduce a mixing proportion $\eta \in [0,1]$; and model the $\omega_{k,k'}$'s as conditionally independently drawn from a Laplace(ξ_1) slab with probability η or a Laplace(ξ_0) spike with probability $(1-\eta)$. We further place independent Exponential(ξ_1) priors on the diagonal elements and truncate the prior to the positive definite cone, yielding the conditional density

$$p(\Omega|\eta) \propto \mathbb{1} (\Omega \succ 0) \times \prod_{k=1}^{q} \xi_1 e^{-\xi_1 \omega_{k,k}} \times \prod_{1 \le k < k' \le q} \left[\eta \xi_1 e^{-\xi_1 |\omega_{k,k'}|} + (1 - \eta) \xi_0 e^{-\xi_0 |\omega_{k,k'}|} \right]$$

To model our uncertainty about the proportion of entries in \boldsymbol{B} and Ω drawn from the slab, we place independent Beta priors on θ and η , so that $p(\theta, \eta) \propto \theta^{a_{\theta}-1} (1-\theta)^{b_{\theta}-1} \times \eta^{a_{\eta}-1} (1-\eta)^{b_{\eta}-1}$, for fixed positive constants $a_{\theta}, b_{\theta}, a_{\eta}$ and b_{η} .

3 Parameter estimation with Monte Carlo Expectation-Conditional Maximization

Following Ročková and George (2018) and Deshpande et al. (2019), we focus on approximating the MAP estimate of $\Xi := (\boldsymbol{B}, \theta, \Omega, \eta)$. Before describing our estimation strategy, we introduce some notation. First, we let $\boldsymbol{X}, \boldsymbol{Y}$, and \boldsymbol{Z} be matrices whose i-th rows are, respectively, $\boldsymbol{x}_i^{\top}, \boldsymbol{y}_i^{\top}$, and \boldsymbol{z}_i^{\top} . Throughout we assume that the columns of $\boldsymbol{X}^{n \times p}$ are centered and scaled to have norm \sqrt{n} . We additionally partition each outcome vector \boldsymbol{y}_i into two parts $\boldsymbol{y}_i^{(C)} \in \mathbb{R}^{q_C}$ which contains the first q_C elements corresponding to the continuous outcomes, and $\boldsymbol{y}_i^{(B)} \in \{0,1\}^{q_B}$, which contains the second q_B elements corresponding to the binary outcomes. We similarly partition each \boldsymbol{z}_i into two parts $\boldsymbol{z}_i^{(C)}$ and $\boldsymbol{z}_i^{(B)}$. Finally we associate each $\boldsymbol{y}^{(B)} = (y_1^{(B)}, \dots, y_{q_B}^{(B)}) \in \{0,1\}^{q_B}$, with an orthant $\mathcal{H}(\boldsymbol{y}^{(B)}) = \{\boldsymbol{z} \in \mathbb{R}^{q_B} : y_k^{(B)} = \mathbb{I}(z_k > 0) \text{ for all } k = 1, 2, \dots, q_B\}$. Thus, under the model in Equation (1), we know that each $\boldsymbol{z}_i \in \mathbb{R}^{q_C} \times \mathcal{H}(\boldsymbol{y}_i^{(B)})$.

For $\Omega \succ 0$, the log posterior density is given by

$$\log p(\boldsymbol{B}, \theta, \Omega, \eta | \boldsymbol{Y}) = \sum_{i=1}^{n} \log p(\boldsymbol{y}_{i} | \boldsymbol{B}, \Omega)$$

$$+ \sum_{j=1}^{p} \sum_{k=1}^{q} \log \left[\theta \lambda_{1} e^{-\lambda_{1} |\beta_{j,k}|} + (1 - \theta) \lambda_{0} e^{-\lambda_{0} |\beta_{j,k}|} \right]$$

$$+ \sum_{1 \leq k < k' \leq q} \log \left[\eta \xi_{1} e^{-\xi_{1} |\omega_{k,k'}|} + (1 - \eta) \xi_{0} e^{-\xi_{0} |\omega_{k,k'}|} \right] - \xi_{1} \sum_{k=1}^{q} \omega_{k,k}$$

$$+ (a_{\theta} - 1) \log \theta + (b_{\theta} - 1) \log (1 - \theta) + (a_{\eta} - 1) \log \eta + (b_{\eta} - 1) \log (1 - \eta).$$
(2)

Directly optimizing the right-hand side of Equation (2) is challenging due to (i) the non-concavity of $\log p(\boldsymbol{B}, \Omega | \theta, \eta)$ (the second and third lines) and (ii) the analytic intractability of the likelihood terms $p(\boldsymbol{y}_i | \boldsymbol{B}, \Omega)$. To overcome these challenges, we deploy a Monte Carlo Expectation-Conditional Maximization algorithm in which we iteratively optimize a surrogate objective formed by approximate marginalization of an augmented posterior distribution. We specifically augment our model with spike-and-slab indicators and latent vectors $\boldsymbol{z}^{(B)}$.

3.1 Tackling non-concavity by augmenting with spike-and-slab indicators

To sidestep the challenges presented by the non-concave penalty term $\log p(\boldsymbol{B}, \Omega | \theta, \eta)$ we follow the general strategy of Deshpande et al. (2019) and augment our model with two collections of binary indicators $\boldsymbol{\delta}^{(\beta)} = \{\delta_{j,k}^{(\beta)} : 1 \leq j \leq p, 1 \leq k \leq q\}$ and $\boldsymbol{\delta}^{(\omega)} = \{\delta_{k,k'}^{(\omega)} : 1 \leq k < k' \leq q\}$. Each $\delta_{j,k}^{(\beta)}$ and $\delta_{k,k'}^{(\omega)}$ encodes whether or not the elements $\beta_{j,k}$ and $\omega_{k,k'}$ are drawn from their respective slab $(\delta = 1)$ or spike $(\delta = 0)$ distributions.

To motivate this approach, first observe that the conditional density of \boldsymbol{B} and Ω can be expressed as

$$p(\boldsymbol{B}, \Omega | \boldsymbol{\theta}, \eta) = \int p(\boldsymbol{B} | \boldsymbol{\delta}^{(\beta)}) p(\boldsymbol{\delta}^{(\beta)} | \boldsymbol{\theta}) d\boldsymbol{\delta}^{(\beta)} \times \int p(\Omega | \boldsymbol{\delta}^{(\omega)}) p(\boldsymbol{\delta}^{(\omega)} | \eta) d\boldsymbol{\delta}^{(\omega)}$$

where each $\delta_{j,k}^{(\beta)}|\theta \sim \text{Bernoulli}(\theta)$ and $\delta_{k,k'}^{(\omega)}|\eta \sim \text{Bernoulli}(\eta)$, independently and

$$p(\boldsymbol{B}|\boldsymbol{\delta}^{(\beta)}) \propto \exp\left\{-\sum_{j=1}^{p} \sum_{k=1}^{q} \left(\lambda_{1} \delta_{j,k}^{(\beta)} + \lambda_{0} (1 - \delta_{j,k}^{(\beta)})\right) |\beta_{j,k}|\right\}$$
$$p(\Omega|\boldsymbol{\delta}^{(\omega)}) \propto \mathbb{1} (\Omega \succ 0) \times \exp\left\{-\xi_{1} \sum_{k=1}^{q} \omega_{k,k} - \sum_{1 \leq k < k' \leq q} \left(\xi_{1} \delta_{k,k'}^{(\omega)} + \xi_{0} (1 - \delta_{k,k'}^{(\omega)})\right) |\omega_{k,k'}|\right\}$$

Based on this representation, an ECM algorithm for approximating the MAP of $\Xi := (\boldsymbol{B}, \theta, \Omega, \eta)$ proceeds by iteratively optimizing a surrogate objective function defined by integrating $\log p(\Xi|\boldsymbol{Y})$ against the conditional posterior distributions of the indicators. Specifically, starting from some initial guess $\Xi^{(0)}$, for t > 1, the t-th iteration of the algorithm consists of an E-step, in which we compute the surrogate objective

$$F^{(t)}(\boldsymbol{B}, \boldsymbol{\theta}, \boldsymbol{\Omega}, \boldsymbol{\eta}) = \mathbb{E}_{\boldsymbol{\delta}^{(\beta)}, \boldsymbol{\delta}^{(\omega)}| \cdot} [\log p(\boldsymbol{\Xi}, \boldsymbol{\delta}^{(b)}, \boldsymbol{\delta}^{(\omega)} | \boldsymbol{Y}) | \boldsymbol{\Xi}^{(t-1)}]$$

and two conditional maximization (CM) steps. In the first CM step, we maximize $F^{(t)}$ with respect to (\boldsymbol{B}, θ) while fixing $(\Omega, \eta) = (\Omega^{(t-1)}, \eta^{(t-1)})$. Then, in the second CM step, we maximize $F^{(t)}$ with respect to (Ω, η) while fixing $(\boldsymbol{B}, \theta) = (\boldsymbol{B}^{(t)}, \theta^{(t)})$.

It is straightforward to verify that the indicators $\delta_{j,k}^{(\beta)}$'s (resp. $\delta_{k,k'}^{(\omega)}$) are conditionally independent given \boldsymbol{B} and $\boldsymbol{\theta}$ (resp. Ω and η). Moreover, their conditional expectations are available in closed form:

$$\mathbb{E}[\delta_{j,k}^{(\beta)}|\boldsymbol{B},\theta] := p_{j,k}^{\star} = \left[1 + \frac{1-\theta}{\theta} \times \frac{\lambda_0}{\lambda_1} \times \exp\left\{-(\lambda_0 - \lambda_1)|\beta_{j,k}|\right\}\right]^{-1}$$

$$\mathbb{E}[\delta_{j,k}^{(\omega)}|\Omega,\eta] := q_{j,k}^{\star} = \left[1 + \frac{1-\eta}{\eta} \times \frac{\xi_0}{\xi_1} \times \exp\left\{-(\xi_0 - \xi_1)|\omega_{k,k'}|\right\}\right]^{-1}$$
(3)

With this notation, the surrogate objective optimized in the t-th iteration of the ECM algorithm is

$$F^{(t)} = \sum_{i=1}^{n} \log p(\mathbf{y}_{i}|\mathbf{B},\Omega) - \sum_{j=1}^{p} \sum_{k=1}^{q} \lambda_{j,k}^{\star} |\beta_{j,k}| - \sum_{1 \le k < k' \le q} \xi_{k,k'}^{\star} |\omega_{k,k'}| - \xi_{1} \sum_{k=1}^{q} \omega_{k,k}$$

$$+ \left(a_{\theta} - 1 + \sum_{j=1}^{p} \sum_{k=1}^{q} p_{j,k}^{\star} \right) \log \theta + \left(b_{\theta} - 1 + pq - \sum_{j=1}^{p} \sum_{k=1}^{q} p_{j,k}^{\star} \right) \log(1 - \theta)$$

$$+ \left(a_{\eta} - 1 + \sum_{1 \le k < k' \le q} q_{k,k'}^{\star} \right) + \left(b_{\eta} - 1 + \frac{q(q-1)}{2} - \sum_{1 \le k < k' \le q} q_{k,k'}^{\star} \right) \log(1 - \eta),$$

$$(4)$$

where $\lambda_{j,k}^{\star} = \lambda_1 p_{j,k}^{\star} + \lambda_0 (1 - p_{j,k}^{\star})$ and $\xi_{k,k'}^{\star} = \xi_1 q_{k,k'}^{\star} + \xi_0 (1 - q_{k,k'}^{\star})$. From the first line of Equation (4), optimizing $F^{(t)}$ with respect to \mathbf{B} or Ω involves solving a maximum likelihood problem with individual penalties ℓ_1 in each entry $\beta_{j,k}$ and $\omega_{k,k'}$. A useful way to view the coefficients $\lambda_{j,k}^{\star}$ and $\xi_{k,k'}^{\star}$ is as entry-specific data-driven penalty levels. Because $p_{j,k}^{\star}$ and $q_{k,k'}^{\star}$ are updated at every E-step according to the current magnitudes of $\beta_{j,k}$ and $\omega_{k,k'}$ (Equation (3)), the effective penalties $\lambda_{j,k}^{\star}$ and $\xi_{k,k'}^{\star}$ adaptively mix between a strong spike (λ_0,ξ_0) and a weak slab (λ_1,ξ_1) . Entries that appear important in the current iterate (i.e., those with large magnitude) receive small penalties in the next CM-step and are allowed to persist, whereas entries close to zero are pushed more aggressively toward exact zero in the next iteration. This adaptive penalty mixing is the key mechanism by which the spike-and-slab LASSO can aggressively shrink negligible parameter values without severely biasing the estimates of truly significant values (see George and Ročková, 2020, for an overview).

3.2 Monte Carlo log-likelihood approximation

Although the augmentation with the spike-and-slab indicators overcomes the challenging non-concave penalty in Equation (2), we cannot compute the surrogate objective $F^{(t)}(\Xi)$ in closed-form. Specifically, observe that for each $i = 1, \ldots, n$,

$$p(\boldsymbol{y}_{i}, \boldsymbol{z}_{i} | \boldsymbol{B}, \Omega) \propto \prod_{k=1}^{q_{c}} \mathbb{1}\left(y_{i}^{(C)} = z_{i}^{(C)}\right) \times \prod_{k=1}^{q_{B}} \mathbb{1}\left(y_{i}^{(B)} = \mathbb{1}\left(z_{i}^{(B)} > 0\right)\right) \times |\Omega|^{\frac{1}{2}} \exp\left\{-\frac{1}{2}\left(\boldsymbol{z}_{i} - \boldsymbol{B}^{\top}\boldsymbol{x}_{i}\right)^{\top} \Omega\left(\boldsymbol{z}_{i} - \boldsymbol{B}^{\top}\boldsymbol{x}_{i}\right)\right\},$$
(5)

To compute $p(y_i|B,\Omega)$, we must integrate the expression on the right-hand side of Equation (5) over the space $\mathbb{R}^{q_c} \times \mathcal{H}(y_i^{(B)})$:

$$p(\boldsymbol{y}_i|\boldsymbol{B},\Omega) = \int_{\mathbb{R}^{q_c}} \int_{\mathcal{H}(\boldsymbol{y}_i^{(B)})} \delta(\boldsymbol{y}_i^{(C)} - \boldsymbol{z}_i^{(C)}) \phi_q(\boldsymbol{z}_i; \boldsymbol{B}^\top \boldsymbol{x}_i, \Omega^{-1}) d\boldsymbol{z}_i^{(B)} d\boldsymbol{z}_i^{(C)},$$

where $\delta(.)$ is the Dirac delta function and $\phi_q(.)$ denotes the standard q-variate Gaussian probability density function. While the outer integral over $\mathbf{z}_i^{(C)}$ is analytically tractable, the inner integral, which involves marginalizing a multivariate Gaussian over an orthant in \mathbb{R}^{q_b} , lacks a closed form expression.

We overcome this challenge by replacing each $\log p(\boldsymbol{y}_i|\boldsymbol{B},\Omega)$ in Equation (4) with a Monte Carlo approximation computed based on sampling the latent \boldsymbol{z}_i 's from their conditional posterior distribution. That is, instead of optimizing $F^{(t)}(\Xi)$ with two CM steps, we instead optimize the objective $\tilde{F}^{(t)}$ which replaces the term $\sum_{i=1}^{n} \log p(\boldsymbol{y}_i|\boldsymbol{B},\Omega)$ in Equation (4) with the quantity $H^{-1}\sum_{i=1}^{n} \sum_{h=1}^{H} \log p(\boldsymbol{y}_i, \boldsymbol{z}_i^{(h)}|\boldsymbol{B},\Omega)$, where H denotes the number of Monte Carlo samples of \boldsymbol{z}_i drawn

Practically, because we know $\mathbf{z}_i^{(C)} = \mathbf{y}_i^{(C)}$, it suffices to sample only the unobserved sub-vector $\mathbf{z}_i^{(B)}$'s. In fact, conditionally on $\mathbf{y}_i, \mathbf{x}_i, \mathbf{B}$, and Ω , $\mathbf{z}_i^{(B)}$ follows a q_b -dimensional multivariate normal distribution truncated to the orthant $\mathcal{H}(\mathbf{y}_i^{(B)})$; see Appendix A.1 for exact expressions for the mean and variance. In our implementation, we use Gessner et al. (2020)'s LinESS algorithm to draw H independent samples of each $\mathbf{z}_i^{(B)}$ using elliptical slice sampling in each iteration of our algorithm.

3.3 Our MCECM algorithm

Formally, our approach is a Monte Carlo ECM (MCECM) algorithm in which we augment our model with the latent z_i 's and the spike-and-slab indicators $\boldsymbol{\delta}^{(\beta)}$ and $\boldsymbol{\delta}^{(\omega)}$. Each iteration of the algorithm involves a Monte Carlo E-step, in which we compute the individual penalties $\lambda_{j,k}^{\star}$ and $\xi_{j,k}^{\star}$ and approximate the log likelihood, and two CM steps, in which sequentially update each of (\boldsymbol{B}, θ) and (Ω, η) while fixing the other.

CM Step 1: updating B **and** θ **.** In the first CM step of the t-th MCECM iteration, we update (B, θ) while fixing $(\Omega, \eta) = (\Omega^{(t-1)}, \eta^{(t-1)})$ by maximizing the function

$$\tilde{F}^{(t)}(\boldsymbol{B}, \boldsymbol{\theta}, \Omega^{(t-1)}, \eta^{(t-1)}) = -\operatorname{tr}\left(\mathbb{M}(\boldsymbol{B})^{\top} \mathbb{M}(\boldsymbol{B}) \Omega^{(t-1)}\right) - \sum_{j=1}^{p} \sum_{k=1}^{q} \lambda_{j,k}^{\star} |\beta_{j,k}|$$

$$+ \left(a_{\theta} - 1 + \sum_{j=1}^{p} \sum_{k=1}^{q} p_{j,k}^{\star}\right) \log \theta + \left(b_{\theta} - 1 + pq - \sum_{j=1}^{p} \sum_{k=1}^{q} p_{j,k}^{\star}\right) \log(1 - \theta),$$

where \mathbb{M} is an $(nh) \times q$ matrix whose rows are $(\boldsymbol{z}_i^{(h)} - \boldsymbol{B}^\top \boldsymbol{x}_i)^\top$. This function is separable in \boldsymbol{B} and $\boldsymbol{\theta}$ and we can update $\boldsymbol{\theta}$ in closed form. Like Deshpande et al. (2019), we update \boldsymbol{B} using cyclic coordinate ascent and use a blend of hard- and soft-thresholding.

To describe the individual $\beta_{j,k}$ updates, we first define the response-wide weighted residuals excluding predictor j: $r_{ik'}^{(-j,h)} = z_{ik'}^{(h)} - \sum_{l \neq j} x_{il} \beta_{lk'}^{(\text{old})}$, where $k' = 1, \ldots, q$. Then, we set $S_{jk} = 1$

 $\sum_{i=1}^{n} \sum_{h=1}^{H} x_{ij} \left(\sum_{k'=1}^{q} \omega_{kk'}^{(t-1)} r_{ik'}^{(-j,h)}\right)$ as the precision-weighted inner product between predictor j and the partial residuals of all responses. Given an existing value $\beta_{j,k}^{\text{old}}$, our cyclical coordinate ascent algorithm iteratively sets

$$\beta_{jk}^{\text{new}} = \left[|S_{jk}| - \lambda_{jk}^{\star} \right] + \frac{\operatorname{sign}(S_{jk})}{nH\omega_{kk}^{(t-1)}} \mathbb{1} \left(\left| \frac{S_{jk}}{nH\omega_{kk}^{(t-1)}} \right| > \Delta_{jk} \right). \tag{6}$$

The elementwise thresholds Δ_{jk} are computed using the same principles detailed in Proposition 2 of Deshpande et al. (2019). To interpret this step, we note that if the absolute score $|S_{jk}|$ is below the data-driven cut-off Δ_{jk}^{\star} , the entry is set exactly to zero. Otherwise, the coefficient is updated by the soft threshold operator with an adaptive penalty of $\lambda_{jk}^{\star}/\omega_{kk}^{(t-1)}$; the penalty is smaller for entries with high posterior slab probability, so truly important effects incur little shrinkage. This dual-threshold mechanism effectively eliminates weak signals and shrinks strong ones, providing a robust yet parsimonious estimator.

CM Step 2: updating Ω and η . After updating \boldsymbol{B} and θ , we update (Ω, η) by maximizing the function

$$F^{(t)}(\boldsymbol{B}^{(t)}, \boldsymbol{\theta}^{(t)}, \Omega, \eta) = \frac{n}{2} \log|\Omega| - \frac{1}{2H} \operatorname{tr}\left(\mathbb{M}(\boldsymbol{B}^{(t)})^{\top} \mathbb{M}(\boldsymbol{B}^{(t)})\Omega\right) - \xi_1 \sum_{k=1}^{q} \omega_{k,k} - \sum_{1 \le k < k' \le q} \xi_{k,k'}^{\star} |\omega_{k,k'}|$$

$$+ \left(a_{\eta} - 1 + \sum_{1 \le k < k' \le q} q_{k,k'}^{\star}\right) + \left(b_{\eta} - 1 + \frac{q(q-1)}{2} - \sum_{1 \le k < k' \le q} q_{k,k'}^{\star}\right) \log(1-\eta)$$

Just like in the first CM step, this objective is separable and we can update η in closed-form. Updating Ω essentially amounts to solving a graphical LASSO problem with individual penalties. In our implementation, we solve this problem using Hsieh et al. (2014)'s QUIC algorithm.

Implementation. Our MCECM algorithm depends on three sets of hyperparameters. The first set are the spike and slab penalties ξ_0, λ_0, ξ_1 , and λ_1 . We recommend setting $\lambda_1 \approx (\sqrt{n \log n})^{-1}$, which induces an amount of shrinkage similar to that induced by the global shrinkage parameter τ in Wang et al. (2025)'s mt-MBSP procedure. We further recommend setting $\xi_1 = n/100$, similar to Deshpande et al. (2019). Instead of fixing single values for the spike penalties λ_0 and ξ_0 , we run our MCECM algorithm along a grid of (λ_0, ξ_0) combinations with warm starts. We vary λ_0 and ξ_0 along grid of ten evenly-spaced values respectively ranging from 10 to 100 and from n/10 and n. In this way, we optimize 100 increasingly spiky posterior distributions, one for each combination of λ_0 and ξ_0 . Such dynamic posterior exploration has proven extremely effective in gradually filtering out negligible parameter values (Ročková and George, 2018; Deshpande et al., 2019).

The hyperparameters a_{θ} , b_{θ} , a_{η} and b_{η} influence the overall sparsity of the outputted solution. Following the suggestions of Shen et al. (2024) and Deshpande et al. (2019), we recommend setting $a_{\theta} = 1$, $b_{\theta} = pq$, and $a_{\eta} = 1$, $b_{\eta} = q$. Finally, we draw H = 2000 realizations of z_i in each MC E-step of our algorithm.

4 Theoretical Results

If the model in Equation (1) is well-specified — that is, if the y_i 's were drawn from that model conditionally on some true data generating parameters B_0 and Ω_0 — then, under mild assumptions

and slight prior modification, the mixed-mSSL posterior concentrates increasingly overwhelming amounts of probability into smaller and smaller neighborhoods around B_0 and Ω_0 as n diverges. In this section, we establish posterior concentration rates for both B (Theorem 3) and Ω (Theorem 6) in the high-dimensional regime where the number of covariates p and the number of outcomes q grow with n. We further demonstrate that as long as the non-zero entries in B_0 are not too small, combining mixed-mSSL with a simple thresholding rule yields a variable selection procedure satisfying the sure screening property (Fan and Lv, 2008), which guarantees high-probability recovery of all non-zero covariate effects.

Like Ročková and George (2018) and Shen and Deshpande (2022), we modify the mixed-mSSL prior and fix the hyperparameters θ and η . This modification simplifies the theoretical analysis without substantially altering the essence of the result. Insofar as our proposed mixed-type model is similar to that studied in Wang et al. (2025) — we both rely on the induced correlation between discrete and continuous outcomes with a latent variable — our theoretical analysis is very similar to theirs. However, that work was limited to the regime in which p grew with n, but q was fixed. Our analysis is much more general and allows q to diverge, albeit at a slower rate than p (viz. $\log p \gtrsim q$). Henceforth, we use p_n and q_n to denote, respectively, the number of covariates and outcomes. We similarly include the subscript n in our notation for the parameters \mathbf{B} and Ω and the matrices \mathbf{X} , \mathbf{Y} , and \mathbf{Z} to indicate that their dimension depends on n. For each $j = 1, \ldots, p_n$, we denote the j-th row of \mathbf{B}_n as \mathbf{b}_j . Finally, we use \mathbb{P}_0 and \mathbb{E}_0 to denote probabilities and expectations taken with respect to the distribution of \mathbf{Y}_n implied by the model in Equation (1) with $\mathbf{B} = \mathbf{B}_0$ and $\Omega = \Omega_0$

4.1 Posterior contraction of *B*

To establish posterior concentration for B, we make the following assumptions:

- (A1) p_n grows sub-exponentially with respect to n and q_n grows polynomially but more slowly than p_n : $n \ll p_n$; $(\log p_n)^2 = o(n)$; and $q_n = n^b$ for some $b \in (0, 1/2)$
- (A2) Let $S_0 = \{j : \text{row } j \text{ of } \mathbf{B}_0 \text{ is non-zero}\}$ be the index of non-zero rows of \mathbf{B}_0 . Then $s_0^B = |S_0| \ge 1$ with $s_0^B = o(n/\log p_n)$.
- (A3) The entries of X_n are uniformly bounded and X has a uniform eigenvalue bound. Specifically there are constants $0 < \underline{\tau} < \overline{\tau} < \infty$ not depending on n such that $||X_n||_{\infty} := \max_{ij} |x_{ij}| \leq \overline{\tau}$ and

$$\inf_{\substack{n \ S \subset \{1, \dots, p_n\}\\ 1 \le |S| < n}} \lambda_{\min} \left(n^{-1} \sum_{i=1}^n \boldsymbol{x}_i^S (\boldsymbol{x}_i^S)^\top \right) > \underline{\tau}.$$

- (A4) The entries of the true B_0 are uniformly bounded. That is, there is a constant a_1 not depending on n such that $||B_0||_{\infty} \leq a_1$.
- (A5) The eigenvalues of Ω_0 are bounded away from 0 and ∞ . That is, there is a constant $k_1 > 0$ not depending on n such that $k_1^{-1} \leq \lambda_{\min}(\Omega_0) < \lambda_{\max}(\Omega_0) < k_1$.
- (A6) The hyperparameters λ_0, λ_1 and θ are such that there exists constants $c, \rho > 0$ not depending on n such that $\mathbb{E}[\|\boldsymbol{b}_j\|_2^2 = cn^{-(1+\rho)}/(p_nq_n)$ for each $j = 1, \ldots, p_n$.

Assumption (A1) allows p_n to grow sub-exponentially with n and for q_n to grow polynomially with n but slower than p_n . Since the quantity s_0^B in Assumption (A2) lower bounds the total number of

non-zero entries in B_0 , Assumption (A2) can be viewed as a restriction on the overall sparsity on B_0 . Assumptions (A3)–(A5) are routinely invoked in the literature (e.g. Castillo et al., 2015; Bai and Ghosh, 2018) and ensure parameter identifiability in the high-dimensional regime we study. Finally, Assumption (A6) ensures that the prior variance of each $\beta_{j,k}$ is of the order $n^{-(1+\rho)}/(p_nq_n)$, which ensures most entries in B_n are shrunk to zero even when q_n diverges.

Lemma 2 is adapted from Lemma D1 in Wang et al. (2025) and we prove it in Appendix A.3. Fundamentally, it shows that the *prior* for B_n concentrates.

Lemma 2 (Prior concentration result for \boldsymbol{B}). Under Assumptions (A1)-(A6), $\mathbb{P}(\|\boldsymbol{B}_n - \boldsymbol{B}_0\|_F < Cn^{-\frac{\rho}{2}}\epsilon_n) > \exp\{-Dn\epsilon_n^2\}$, where $\epsilon_n^2 = n^{-1}\max\{q_n, s_0^B\}\log p_n$ and $C, \rho, D > 0$ are constants not depending on n.

This result, which is a foundational part of our analysis, shows that as $n \to \infty$, the prior concentrates increasing amounts of probability mass in a Frobenius-norm ball around the true \mathbf{B}_0 of vanishing radius. Theorem 3 shows that the rate $\epsilon_n = \left(n^{-1} \max\{q_n, s_0^B\} \log p_n\right)^{\frac{1}{2}}$ in Lemma 2 is also the posterior contraction rate.

Theorem 3 (Posterior unconditional contraction result for B). Under Assumptions (A1)–(A6), for any constant M > 0, as $n \to \infty$, we have

$$\sup_{\boldsymbol{B}_0} \mathbb{E}_0 \left[\mathbb{P} \left(\| \boldsymbol{B}_n - \boldsymbol{B}_0 \|_F > M \epsilon_n | \boldsymbol{Y}_n \right) \right] \to 0,$$

where $\epsilon_n^2 = n^{-1} \max\{q_n, s_0^B\} \log p_n$.

We prove Theorem 3 in Appendix A.5 in two steps. First, we show that the posterior concentrates conditionally given the data Y_n and the latent variable Z_n (Lemma 4). Because it conditions on the unobservable Z_n , this result is weaker than traditional posterior contraction¹.

Lemma 4 (Posterior conditional contraction result for B). Under the Assumptions (A1) – (A6), for any arbitrary constant M > 0 and ϵ_n^2 as in Lemma 2, $\sup_{B_0} \mathbb{E}_0 \left[\mathbb{P} \left(\| \mathbf{B}_n - \mathbf{B}_0 \|_F > M \epsilon_n | \mathbf{Y}_n, \mathbf{Z}_n \right) \right] \to 0$, as $n \to \infty$

Next, we remove the conditioning on Z_n using a conventional "good set" argument (Ash and Doleans-Dade, 2000, Chapter 1). To elaborate, we let $\mu_i = B^{\top} x_i \in \mathbb{R}^{q_n}$ denote the mean of the latent variables for each $i = 1, \ldots, n$ and define the "good set"

$$\mathcal{Z}_n = \left\{ (z_{ik}) : \max_{i,k: y_{ik} \text{ binary}} \left| z_{ik} - \mu_{ik} \right| \le C_0 \sqrt{\log n} \text{ and } \max_{i,k: y_{ik} \text{ continuous}} \left| z_{ik} \right| \le M_0 \right\}, \quad (7)$$

where $C_0 > 0$ is suitably large, and $M_0 > 0$ is a uniform bound for y_{ik} if the response is continuous. Informally, \mathcal{Z}_n excludes extreme or pathological latent draws that deviate too far from their means for binary responses (i.e., $|z_{ik} - \mu_{ik}| > C_0 \sqrt{\log n}$) or exceed a suitable bound for continuous $z_{ik} = y_{ik}$.

Lemma 5 crucially shows that almost all posterior probability resides in \mathcal{Z}_n .

Lemma 5 (High-probability lemma for good sets). Under Assumptions (A1)-(A5), there exists a sequence $\delta_n \to 0$ such that $\mathbb{P}(\mathbf{Z}_n \notin \mathcal{Z}_n | \mathbf{Y}_n) \leq \delta_n$ with high \mathbb{P}_0 -probability.

¹Our result is, however, similar in spirit to Theorem 3 of Zito and Miller (2024), which also establishes posterior contraction conditional on an auxiliary latent variable in a non-negative matrix factorization model.

It turns out that Lemma 4 essentially holds uniformly for all $\mathbf{Z}_n \in \mathcal{Z}_n$. Thus, marginalizing over $\mathbf{Z}_n \in \mathcal{Z}_n$ yields the desired unconditional contraction result. Combining this result with the sequence of arguments in Lemma 2 and Lemma 4 demonstrate how posterior contraction, initially conditional on latent variables, can be rigorously extended to an unconditional form. The lemma 5 is conceptually identical to Proposition C.7 of Wang et al. (2025), which shows that if a posterior event has asymptotically vanishing probability when we condition on the *latent* augmented variables \mathbf{Z} , then it also has vanishing probability when we condition on the *observed* data \mathbf{Y} , and conversely for events whose probability stays bounded away from 0.

Before proceeding, we pause to compare our $\epsilon_n^2 = n^{-1} \max\{q_n, s_0^B\} \log p_n$ to other rates reported in the literature for similar problems. When q is fixed and does not grow with n, $\max\{q_n, s_0^B\} = s_0^B$ and our squared rate simplifies to $n^{-1}s_0^B \log p_n$, which exactly matches the rate reported in Theorem 3.1 of Wang et al. (2025). Shen and Deshpande (2022) studied a special case of our problem that featured only continuous outcomes and no binary outcomes. In that setting, they obtained a squared rate of $n^{-1} \max\{q_n, s_0^B\} \log(\max\{p_n, q_n\})$. Because we allow p_n to grow much faster than q_n (Assumption (A1)), we have $\log(\max\{p_n, q_n\}) = \log p_n$, which shows that our rate coincides exactly with theirs.

4.2 Posterior contraction of Ω

Our analysis of the mixed-mSSL posterior for Ω requires additional assumptions and modifications to the prior. Specifically, in addition to assuming that the true precision matrix has eigenvalues bounded away from zero and infinity, we additionally assume that it has at most s_0^{Ω} non-zero off-diagonal entries in its upper triangle. That is, we assume Ω_0 lies in the space

$$\mathcal{U}(k_1, s_0^{\Omega}) = \left\{ \Omega \in \mathcal{M}_{q_n}^+(k_1) : \sum_{k < k'} \mathbb{1} \left(\omega_{k, k'} \neq 0 \right) \le s_0^{\Omega} \right\},\,$$

for some $s_0^{\Omega} \geq 1$ where k_1 is as in Assumption (A5) and for any $\lambda > 0$ the space $\mathcal{M}_{q_n}^+(\lambda)$ is defined as

$$\mathcal{M}_{q_n}^+(\lambda) = \{\Omega \succ 0 : \lambda^{-1} \le \lambda_{\min}(\Omega) \le \lambda_{\max}(\Omega) < \lambda\}.$$

We additionally modify the prior over Ω_n so that initial element-wise prior is truncated to the space $\mathcal{M}_{q_n}^+(k_1)$ instead of the whole positive definite cone. We additionally assume

- (B1) The number of outcomes $q_n = n^{-b}$ for some $b \in (0, 1/2)$ and the effective complexity of Ω_0 obeys $n^{-1}(q_n + s_0^{\Omega}) \log q_n = o(1)$.
- (B2) $\eta < q_n^{-a}$ for some fixed a > 0 not depending on n.

We believe that Assumption (A1) and (B1)'s assumption that q_n grows slower than \sqrt{n} is critical. Indeed, arguments in Sarkar et al. (2025) suggest that relaxing the assumption to allow $q_n/n \to \gamma < \infty$ would lead to posterior inconsistency. Assumption (B2) ensures the mixed-mSSL prior puts sufficient mass around the true zero elements in the precision matrix. It is worthwhile to note that enforcing $\sigma_k^2 = 1$ for $k = q_c + 1, \ldots, q$ does not invalidate Assumption (A5) since diagonal inflation (or deflation) by a bounded factor only shifts the spectrum within a bounded interval.

Theorem 6 (Posterior unconditional contraction result for Ω). Under Assumptions (A5), (B1), and (B2), for a sufficiently large constant M > 0, $\sup_{\Omega_0} \mathbb{E}_0 \mathbb{P}(\|\Omega_n - \Omega_0\|_F > M\tilde{\epsilon}_n | \mathbf{Y}_n) \to 0$ where

 $\tilde{\epsilon}_n^2 = n^{-1}(q_n + s_0^{\Omega}) \log q_n$ and s_0^{Ω} denotes the number of non-zero off-diagonal elements in the upper-triangle of Ω .

We prove Theorem 6 in Appendix A.6 using an essentially similar argument as with Theorem 3: we first show that the contraction holds conditionally given Z_n (Lemma A2) and then employ a "good set" argument to remove the conditioning. The rate of posterior contraction in Theorem 6 agrees with the optimal posterior contraction rate established by Banerjee and Ghosal (2015, Theorem 3.1) for Bayesian graphical LASSO and by Zhang et al. (2022, Theorem 2) for graphical horseshoe in precision matrix estimation problems.

The rates ϵ_n and $\tilde{\epsilon}_n$ are fully compatible. When q_n dominates the sparsity levels (i.e., $q_n \gg s_0^B, s_0^\Omega$), both quantities shrink at essentially the same order $\sqrt{(q_n \log n)/n}$, differing only by the two separate logarithmic factors, $\log p_n$ versus $\log q_n$). On the other hand, when the signal-sparsity dominates (i.e., $s_0^B \gg q_n$ but $s_0^\Omega \ll q_n$), the two rates adapt automatically: the **B**-rate (ϵ_n) is driven by s_0^B , whereas the Ω -rate (i.e., $\tilde{\epsilon}_n$) is driven by q_n . Hence each component contracts at the fastest possible rate permitted by its own sparsity level. Finally, in the mixed regime, both rates are governed by $\max\{q_n, s_0^B\}$ or $q_n + s_0^\Omega$, respectively, again reflecting the minimal effective dimension of each matrix.

4.3 Variable selection consistency

Although Theorem 3 implies that we can consistently estimate B_0 with mixed-mSSL, it does not speak to our ability to recover B_0 's support (i.e., the set $S_0 = \{(j,k) : (B_0)_{j,k} \neq 0\}$). Because we use absolutely continuous priors, the mixed-mSSL will generally place all of its posterior probability on dense matrices B_n , all of whose entries are non-zero. Similar to Song and Liang (2023) and Wei and Ghosal (2020) and inspired by Ročková and George (2018)'s notion of generalized dimension, we can threshold the entires of B_n to estimate S_0 . Specifically, given any B_n and Ω_n , let \widetilde{B}_n be the $p_n \times q_n$ matrix obtained by thresholding B_n element-wise as $\widetilde{\beta}_{j,k} = \beta_{j,k} \mathbb{1} (|\beta_{j,k}| > a_n \omega_{k,k})$, where $a_n^2 = (c^2 \log p_n)/(np_n^2)$ for some constant c > 0. Let $\widetilde{S}_n = \{(j,k) : \widetilde{\beta}_{j,k} \neq 0\}$ be the support of \widetilde{B}_n .

In order to study the posterior distribution of \tilde{S}_n , we assume that \mathbf{B}_0 satisfies a mild "beta-min" condition, which ensures all non-zero entires in \mathbf{B}_0 are large enough to be distinguished from zero.

(C1) There are constants $c_3 > 0$ and $0 < \zeta < 1/4$, such that $|(\boldsymbol{B}_0)_{j,k}| > c_3 n^{-\zeta}$ for all $(j,k) \in S_0$.

Theorem 7 (Sure screening via hard thresholding). Under Assumptions (A1), (A2), (B1), and (C1), the sure screening property holds in the sense that, as $n \to \infty$, $\sup_{B_0} \mathbb{E}_0 \mathbb{P}(S_0 \subset \tilde{S}_n | \mathbf{Y}_n) \to 1$.

We emphasize that Theorem 7 does not guarantee perfect model selection, as it allows for the possibility of false positives. However, the sure screening property does provide a strong theoretical guarantee about the number of false negatives that mixed-mSSL can make, provided that the entries of B_0 are large enough.

5 Synthetic Experiments

We performed a simulation study to evaluate how well mixed-mSSL can recover the supports of \boldsymbol{B} and Ω in finite data settings. We simulated several synthetic datasets of varying dimensions and with varying sparsity patterns. We compared mixed-mSSL to three competitors: Wang et al.

(2025)'s mt-MBSP, and two baseline methods, sepSSL and sepglm. The method sepSSL fits a SSLASSO model to each outcome separately, using the standard continuous-outcome version of Ročková and George (2018)'s spike-and-slab LASSO for continuous outcomes and a probit version of spike-and-slab LASSO for binary outcomes. The second baseline method, sepglm, separately fits penalized generalized linear models (GLMs) to each outcome, using a Gaussian model with LASSO penalty for continuous outcomes, and a binomial probit model with LASSO penalty for binary outcomes, both implemented using glmnet (Friedman et al., 2010). Like mixed-mSSL, mt-MBSP jointly models mixed-type outcomes using a latent regression formulation, but unlike mixed-mSSL, mt-MBSP specifies element-wise horseshoe priors (Carvalho et al., 2009) on the matrix of regression coefficients and an inverse Wishart prior on the residual latent precision matrix. It is worth mentioning that we did not include the mmrr method of Ekvall and Molstad (2022) as it requires the number of observations (n) to exceed the number of covariates (p), while our simulation settings specifically focus on the more challenging regime where p > n.

We simulated data for three different dimensions (n, p, q) = (200, 500, 4), (500, 1000, 4), and (800, 1000, 6). For each choice of (n, p, q) we set $q_B = q_C = q/2$ so that half of the outcomes are continuous and the other half are binary. Like Shen et al. (2024), we constructed six different Ω for each (n, p, q): (i) an AR(1) model for Ω^{-1} so that Ω is tri-diagonal; (ii) an AR(2) model for Ω^{-1} so that $\omega_{k,k'} = 0$ whenever |k - k'| > 2; (iii) a setting where Ω is block diagonal with two dense $q/2 \times q/2$ diagonal blocks; (iv) a star graph where the off-diagonal entry $\omega_{k,k'} = 0$ except the case when k or k' is equal to 1; (v) a small-world network; and (vi) a tree network. We defer specific details about these constructions to Appendix B.1 of the Supplementary Materials.

For each (n, p, q), we drew the rows of the design matrix X independently from a $\mathcal{N}_p(\mathbf{0}, \Gamma)$ distribution where the (j, j') entry of Γ is $0.5^{|j-j'|}$. We considered two different settings of \mathbf{B} , each containing 30% non-zero entries. In the first setting, we drew the non-zero entries uniformly from the interval [-5, 5] while in the second setting we drew non-zero entries uniformly from the set $[-5, -2] \cup [2, 5]$. For each combination of (\mathbf{B}, Ω) we generated 100 synthetic datasets from the model in Equation (1).

We ran mixed-mSSL with the default hyperparameter settings described in Section 3. In our experiments, we used the MAP estimate corresponding to the largest spike penalties as point estimates for \boldsymbol{B} and Ω . For sepSSL, we assembled a point estimate of \boldsymbol{B} column-by-column using the MAP estimates corresponding to the largest spike penalties returned by univariate SSLASSO fits using the default settings recommended by Ročková and George (2018). For mt-MBSP, we took the posterior-median matrix as the point estimate of \boldsymbol{B} and treated an entry as non-zero whenever the associated marginal 95% posterior credible interval excluded zero. Similar to sepSSL, sepglm separately fits penalized generalized linear models to each outcome using cross-validated glmnet; \boldsymbol{B} is obtained by simply concatenating the q estimated column vectors. Note that sepSSL and sepglm do not return estimates of Ω , and mt-MBSP generally does not return a sparse estimate of Ω .

It is important to note that mixed-mSSL, sepSSL and sepglm target the same matrix of regression coefficients B from Equation (1). By contrast, mt-MBSP employs an inverse-Wishart prior on Ω^{-1} , which implicitly averages over the unknown latent variances and thus produces regression coefficients on a fundamentally different scale. Because of these differences in interpretation, we do not report parameter estimation errors. Instead, we focus on support recovery metrics (sensitivity,

specificity, precision, and accuracy), which are invariant to scale and assess each method's ability to recover the sparsity patterns in \mathbf{B} and Ω , providing a basis for a fairer comparison.

To complement support recovery, we also assess each method's predictive performance on held-out test data, using metrics that are model-agnostic and naturally comparable. Specifically, we considered regression-function error (RFE), predictive root mean square error (RMSE) averaged over the continuous outcomes, and the mean area under the ROC curve (AUC) for the binary outcomes. For a test sample of size n/2, to calculate RFE, we first evaluated the true conditional means $\mathbb{E}[Y|X]$ at test covariate values using the true parameters and compared these with the estimates provided by each method, taking the average vector ℓ_2 norm between predicted and true conditional means. The predictive RMSE was computed by first generating new test outcomes from the true model and, for each method, generating corresponding predictions using samples from its fitted model and then comparing these predicted values to the true test outcomes, while AUC was obtained by comparing the predicted probabilities to the observed binary outcomes.

Table 1 summarizes estimation and predictive performance for different covariance structures with (n, p, q) = (200, 500, 4) under the signal setting $\mathcal{U}[-5, 5]$. The best results achieved by the method(s) for each scenario are bold-faced. Across all scenarios, mixed-mSSL consistently delivered superior predictive performance, achieving the lowest regression-function error (RFE), predictive root mean square error (RMSE), and the highest area under the ROC curve (AUC). Notably, while sepglm exhibited the highest sensitivity (SEN), it frequently had lower specificity (SPEC) and accuracy (ACC) compared to mixed-mSSL and mt-MBSP. The latter two methods, particularly mt-MBSP, consistently showed high SPEC and precision (PREC), suggesting conservative but reliable detection of true signals. sepSSL generally provided fast computations but was marked by lower PREC and SPEC, indicating a tendency toward higher false-positive identifications. The high precision of mt-MBSP is expected given its very low sensitivity, leading to fewer false positives.

The leftmost panel in Figure 1 shows a histogram of the $\beta_{j,k}$ values for mixed-mSSL's true positive (blue) and false negative (red) identifications from a single replication from the AR(1) setting. This histogram points to the source of mixed-mSSL's low sensitivity in the $\mathcal{U}[-5,5]$ signal scenario: mixed-mSSL simply has limited power to detect very small signals when n is small. To investigate this phenomenon further, we kept \mathbf{B} and Ω fixed and increased the number of observations from n = 200 to n = 500 and n = 800. As we increased n, we found that the distribution of $\beta_{j,k}$ values corresponding to mixed-mSSL's false non-identifications concentrate into smaller and smaller neighborhoods around zero. That is, mixed-mSSL's ability to identify small non-zero signals improved markedly as we increased n, which is exactly anticipated by Theorem 7.

Table 2 summarizes estimation and predictive performance results for signals drawn from the disjoint interval $\mathcal{U}[-5,-2] \cup [2,5]$. This setting is relatively less challenging compared to the previous scenario, where signals were typically concentrated around zero. Consequently, we observe that mixed-mSSL's sensitivity (SEN) notably improves. mt-MBSP consistently achieves high specificity (SPEC) and precision (PREC), albeit with relatively lower sensitivity. On the other hand, sepSSL and sepglm exhibit higher sensitivity but at the cost of lower specificity and precision, indicating more frequent false positives. mixed-mSSL demonstrates an optimal balance, substantially improving sensitivity without a large sacrifice in specificity, precision, or accuracy (ACC). Specifically, it attains competitive predictive performance metrics across all covariance structures, evidenced by consistently low regression-function error (RFE), predictive RMSE, and the highest mean area under

Table 1: Support recovery and predictive performance across different covariance structures with (n, p, q) = (200, 500, 4) under the signal setting $\mathcal{U}[-5, 5]$.

Scenario	Method		Support	recovery	7		P	redictive	;
Scellario	Method	SEN	SPEC	PREC	ACC	TIME(s)	$\overline{\mathbf{RFE}}$	RMSE	AUC
	mt-MBSP	0.10	0.97	0.63	0.71	205.13	43.89	1.78	0.58
AR1	sepSSL	0.31	0.83	0.45	0.68	0.37	43.69	1.14	0.53
	sepglm	0.40	0.81	0.48	0.68	1.74	43.55	0.71	0.58
	mixed-mSSL	0.21	0.91	0.52	0.70	18.26	43.46	0.69	0.61
	mt-MBSP	0.10	0.97	0.62	0.71	146.10	43.89	1.78	0.58
AR2	sepSSL	0.31	0.84	0.44	0.67	0.40	43.70	1.15	0.52
	sepglm	0.41	0.81	0.48	0.68	1.57	43.56	0.71	0.57
	mixed-mSSL	0.21	0.92	0.52	0.72	24.62	43.47	0.70	0.61
	mt-MBSP	0.11	0.97	0.63	0.71	198.61	43.89	1.77	0.58
Block Diagonal	sepSSL	0.31	0.83	0.44	0.67	0.36	43.69	1.14	0.53
	sepglm	0.40	0.81	0.48	0.69	1.71	43.56	0.72	0.58
	${\tt mixed-mSSL}$	0.21	0.91	0.53	0.71	21.53	43.47	0.69	0.60
	mt-MBSP	0.10	0.98	0.63	0.71	186.66	43.89	1.78	0.58
Star Graph	sepSSL	0.32	0.84	0.45	0.67	0.34	43.69	1.14	0.53
	sepglm	0.41	0.81	0.48	0.68	1.63	43.55	0.71	0.58
	${\tt mixed-mSSL}$	0.22	0.91	0.52	0.71	22.40	43.47	0.70	0.61
	mt-MBSP	0.11	0.97	0.63	0.71	183.06	43.89	1.78	0.58
Small World	sepSSL	0.31	0.83	0.44	0.67	0.33	43.69	1.14	0.53
	sepglm	0.40	0.81	0.48	0.68	1.58	43.55	0.71	0.58
	mixed-mSSL	0.21	0.91	0.54	0.70	28.97	43.47	0.70	0.61
	mt-MBSP	0.10	0.97	0.62	0.71	189.30	43.89	1.78	0.58
Tree Network	sepSSL	0.31	0.83	0.45	0.67	0.34	43.69	1.14	0.53
	sepglm	0.41	0.81	0.48	0.69	1.63	43.55	0.71	0.58
	mixed-mSSL	0.22	0.91	0.53	0.71	24.40	43.47	0.70	0.61

the ROC curve (AUC).

Table B1 reports mixed-mSSL's support recovery performance for Ω across the various covariance structures. Because mt-MBSP typically returns a dense Ω (thanks to its use of an inverse Wishart prior), rendering it uninformative for evaluating support recovery or variable selection performance. Qualitatively similar results for other settings are presented in Appendix B of the Supplementary Materials.

6 Real Data Analysis

In this section, we demonstrate mixed-mSSL's performance in settings with large n (Section 6.1), large p (Section 6.2), and large q (Section 6.3).

Table 2: Support recovery and predictive performance across different covariance structures with (n, p, q) = (200, 500, 4) under the disjoint signal setting $\mathcal{U}[-5, -2] \cup [2, 5]$.

Scenario	Method		Support	recovery	7		Predictive		
Scenario	Method	SEN	SPEC	PREC	ACC	TIME(s)	$\overline{ ext{RFE}}$	RMSE	AUC
	mt-MBSP	0.10	0.96	0.57	0.70	133.44	54.94	1.78	0.58
AR1	sepSSL	0.31	0.83	0.44	0.67	0.34	54.79	1.17	0.52
	sepglm	0.39	0.81	0.48	0.69	1.45	54.70	0.80	0.58
	mixed-mSSL	0.35	0.86	0.51	0.70	31.49	54.57	0.77	0.60
	mt-MBSP	0.11	0.96	0.58	0.70	151.87	54.94	1.78	0.57
AR2	sepSSL	0.32	0.83	0.45	0.67	0.41	54.79	1.17	0.53
	sepglm	0.39	0.81	0.48	0.69	1.70	54.70	0.80	0.57
	mixed-mSSL	0.36	0.85	0.50	0.71	19.95	54.57	0.78	0.61
	mt-MBSP	0.10	0.96	0.57	0.70	136.08	54.94	1.78	0.58
Block Diagonal	sepSSL	0.31	0.83	0.45	0.68	0.35	54.79	1.17	0.52
	sepglm	0.39	0.82	0.48	0.69	1.47	54.70	0.80	0.57
	${\tt mixed-mSSL}$	0.35	0.85	0.49	0.69	29.22	54.58	0.78	0.60
	mt-MBSP	0.10	0.96	0.57	0.70	124.39	54.94	1.78	0.58
Star Graph	sepSSL	0.31	0.83	0.45	0.68	0.34	54.80	1.18	0.53
	sepglm	0.38	0.82	0.48	0.69	1.40	54.69	0.80	0.58
	${\tt mixed-mSSL}$	0.35	0.86	0.52	0.71	30.77	54.58	0.78	0.61
	mt-MBSP	0.10	0.96	0.57	0.70	204.06	54.94	1.78	0.58
Small World	sepSSL	0.31	0.83	0.44	0.67	0.36	54.79	1.17	0.52
	sepglm	0.39	0.81	0.48	0.69	1.74	54.71	0.81	0.57
	${\tt mixed-mSSL}$	0.34	0.85	0.51	0.69	26.23	54.58	0.78	0.60
	mt-MBSP	0.11	0.97	0.58	0.70	196.86	54.94	1.78	0.57
Tree Network	sepSSL	0.32	0.83	0.44	0.67	0.35	54.80	1.17	0.53
	sepglm	0.39	0.82	0.49	0.69	1.70	54.70	0.80	0.57
	${\tt mixed-mSSL}$	0.35	0.84	0.53	0.70	23.64	54.57	0.77	0.61

6.1 Chronic Kidney Disease Data

Our first motivating dataset comes from Ebiaredoh-Mienye et al. (2022), which identified important biomarkers for chronic kidney disease (CKD). The dataset contains measurements from n=400 patients. For each patient, we observe two outcomes, an indicator of whether they have CKD and their urine-specific gravity (SG), a continuous measurement of the concentration of waste products in urine. We further observe p=24 covariates, which include the results from several clinical lab tests (e.g., albumin, hemoglobin, and random blood glucose) and indicators of other health conditions (e.g., diabetes, hypertension, anemia, coronary artery disease). Ebiaredoh-Mienye et al. (2022) identified 10 covariates as significantly predictive of CKD status. In our re-analysis, we compared how well mixed-mSSL, mt-MBSP, sepSSL, and sepglm recovered these known biomarkers and predicted CKD status and SG. Although this dataset lies in the classical regime where n > p,

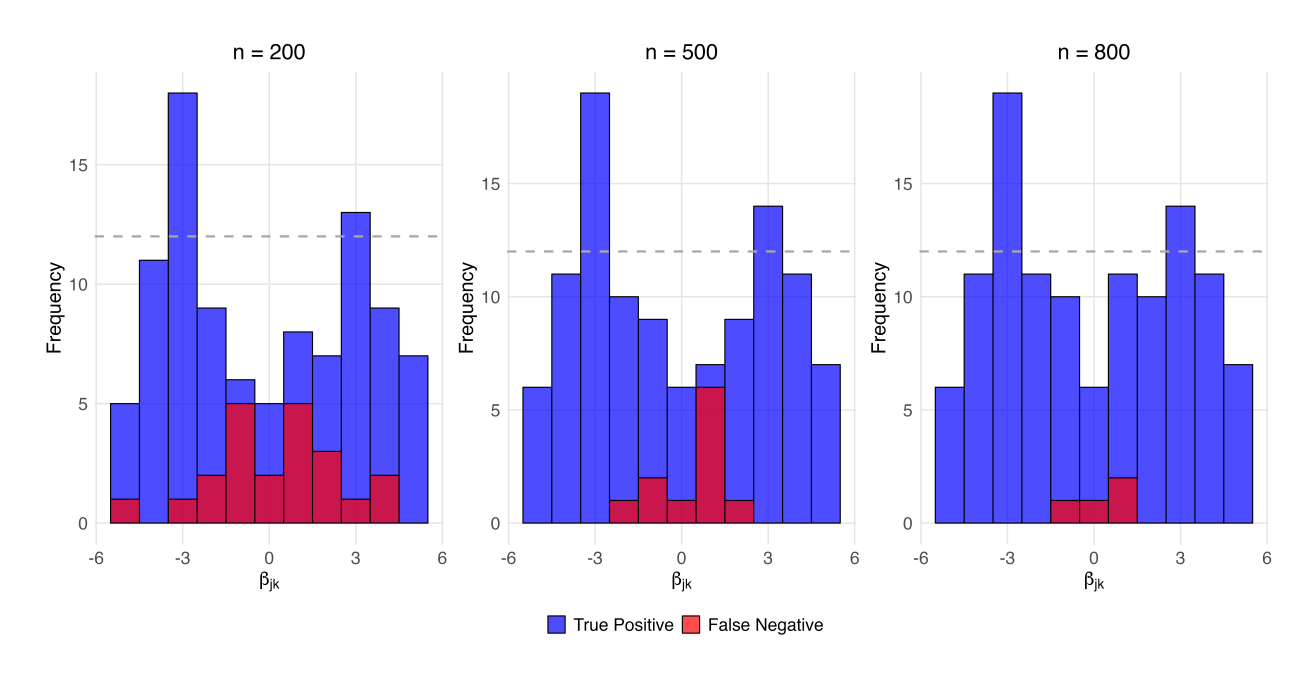


Figure 1: Variation of sensitivity for mixed-mSSL as the sample size n increases for fixed p,q.

the mmrr method failed to converge during model fitting and consequently threw errors, preventing its inclusion in our comparison.

Table 3 summarizes variable selection performance for CKD. All methods consistently identified three key biomarkers: albumin, hemoglobin, and diabetes; see Table C1 for the full list of selected variables. mixed-mSSL identified six of the 10 biomarkers with the highest precision (0.86), accuracy (0.79), and specificity (0.93), indicating excellent balance between false positives and false negatives. In contrast, mt-MBSP and sepSSL were more conservative, each identifying only four true biomarkers, with sepSSL having lower specificity and precision due to additional false positives. On the other hand, sepglm selected significantly more biomarkers (16 in total) and achieved the highest sensitivity (0.90) but substantially lower specificity (0.50) and accuracy (0.56), highlighting a trade-off between identifying true biomarkers and introducing false positives.

Interestingly, mixed-mSSL and sepglm were the only methods to identify random blood glucose (BGR) as an important predictor of CKD status. Previous studies (e.g., Kumar et al., 2023; Hassanein and Shafi, 2022) have corroborated this association, noting that elevated blood glucose can increase blood pressure, placing additional strain on the kidneys and accelerating kidney damage.

We additionally compared each method's predictive performance using five-fold cross-validation. We assessed predictive performance for CKD using the area under the receiver operating characteristic curve (AUC) and for SG using RMSE. Across five-folds, mixed-mSSL had the highest AUC for classifying CKD status (0.993 versus 0.972 for mt-MBSP, 0.967 for sepSSL and 0.988 for sepglm) and the lowest RMSE for predicting SG (4.33 \times 10⁻³ versus 4.44 \times 10⁻³ for mt-MBSP, 4.63 \times 10⁻³ for sepSSL, and 4.52 \times 10⁻³ for sepglm).

Table 3: Classification performance of different methods for detecting the 10 gold-standard CKD biomarkers.

Method	# Selected	SEN	SPEC	ACC	PREC
mixed-mSSL	7	0.60	0.93	0.79	0.86
mt-MBSP	5	0.40	0.93	0.71	0.80
sepSSL	6	0.40	0.86	0.67	0.67
sepglm	16	0.90	0.50	0.56	0.67

6.2 Colorectal Cancer Data

To illustrate the utility of mixed-mSSL in a high-dimensional setting with $p \gg n$, we revisited the pooled gut-metagenomic compendium of five colorectal-cancer (CRC) cohorts (Zeller et al., 2014; Feng et al., 2015; Yu et al., 2017; Vogtmann et al., 2016; Wirbel et al., 2019). After harmonization and removal of missing covariates, the working data consists of n=286 subjects and the relative abundances of p=401 bacterial species that are present in at least 20% of samples. For each subject, we observe q=3 outcomes: a binary indicator of CRC; a binary indicator of Type-2 Diabetes; and the Body Mass Index (BMI). Joint analysis of these three outcomes is biologically motivated as obesity and diabetes are well-established risk modifiers for CRC and share overlapping microbiome signature (Qin et al., 2012; Mandic et al., 2024).

Using mixed-mSSL, we identified five taxa as protective (i.e., the corresponding $\beta_{j,k}$'s were negative) and five as risk factors (i.e., the corresponding $\beta_{j,k}$'s were positive) for CRC. Blautia wexlerae and Anaerotipes hadrus — both prominent butyrate producers — were identified as protective; reduced levels of these taxa have been consistently observed in CRC patients relative to healthy controls (Louis et al., 2014; Kostic et al., 2013). By contrast, Ruminococcus torques, Clostridium citroniae, Alistipes indistinctus, and Oscillibacter spp. were all positively associated with CRC risk by mixed-mSSL; prior studies have reported over-representation of these anaerobes in tumor tissue or stool from CRC cohorts, suggesting pro-inflammatory or genotoxic roles (Zeller et al., 2014; Liu et al., 2023).

mixed-mSSL identified a single Clostridial cluster member (Clostridium sp.) as having a nominally protective effect against Type-2 diabetes. This finding aligns with previous murine studies showing that this species is involved in short-chain fatty acid synthesis and improved insulin sensitivity (Razavi et al., 2024). mixed-mSSL also identified Bacteroides vulgatus and certain Clostridiales spp. as risk factors for diabetes, consistent with metagenomic surveys that report enrichment of these taxa in hyperglycemic individuals (Qin et al., 2012; Karlsson et al., 2013). Turning to Ω , mixed-mSSL recovered very small negative partial correlations (-0.008) between diabetes and CRC status, suggesting that having a latent risk for one disease barely decreases the risk of the other, after accounting for the covariates and BMI. It also identified a very small positive partial correlation (0.011) between BMI and diabetes and a small negative partial correlation between BMI and CRC risk.

Compared to mixed-mSSL, sepSSL identified far fewer taxa (1) as predictive of CRC and diabetes status while mt-MBSP and sepglm identified many more: (72) and (90) respectively. Because we lacked a gold standard set of significant taxa against which to assess these identifications, we

performed another predictive comparison using five-fold cross-validation. Similar to our analysis of the CKD data, we assessed each method's ability to predict binary outcomes using AUC and continuous outcomes using RMSE. For discriminating between CRC cases and controls, mixed-mSSL had the highest AUC (0.774 compared to 0.722 for mt-MBSP, 0.6011 for sepSSL, and 0.6929 for sepglm). It similarly performed the best at predicting diabetes status, achieving an AUC of 0.614 compared to mt-MBSP's 0.585, sepSSL's 0.529, and sepglm's 0.566 and BMI, displaying a much lower an RMSE (4.133) than mt-MBSP (4.813), sepSSL (19.511), and sepglm (6.577). Taken together, these results suggest that mixed-mSSL was better able to share information across related outcomes than mt-MBSP, yielding better predictions with fewer covariates.

6.3 Finnish Bird Data

We finally demonstrate mixed-mSSL's utility in settings with only binary outcomes by re-analyzing a dataset containing yearly counts of the q=50 most common Finnish breeding birds present at n=137 locations that were originally compiled by Lindström et al. (2015) and later analyzed by Ovaskainen and Abrego (2020). We focus on a single survey year (2014) and let $Y_{i,k}=1$ if the number of birds of species k observed at site i exceeds that species' median count across all sites in 2013, and $Y_{i,k}=0$ otherwise. The dataset contains measurement of p=4 covariates at each location: the average temperatures in April & May; the effort (in hours) expended by the observer to survey the location; the average temperature in June & July; and the average winter temperature. mixed-mSSL selected the temperature variables as the most relevant predictor of whether most species were present in greater abundance at a site in 2014 than in 2013.

More interesting, ecologically, is the estimated precision matrix Ω . Recall that latent residual dependencies captured by Ω induce dependence between the observed outcomes. Figure 2 shows a network whose vertices correspond to species and whose edges correspond to non-zero off-diagonal elements in the upper triangle of Ω . Edges corresponding to positive $\omega_{k,k'}$ values are colored black and suggest a positive partial correlation — that is, the two species tend to co-occur at the same location more often than expected based on the covariates and presence of other species. Edges corresponding to negative $\omega_{k,k'}$ values, which indicate negative partial correlations, are colored red. The widths of the edges in Figure 2 are proportional to $|\omega_{k,k'}|$, with thicker lines indicating larger partial correlations. In Figure 2, we observe a single positive partial correlation between Turdus-iliacus (redwing) with Gallinago-qallinago (common snipe). These two species often share wet, rush-dominated meadows and bog margins in boreal Finland. The positive edge recovered by mixed-mSSL plausibly reflects a real tendency for these species to co-occur after climatic effects are removed (Virkkala and Lehikoinen, 2014). In contrast, the abundance of negative edges among woodland versus farmland species (e.g., Columba-palumbus and Sylvia-borin opposing Emberizacitrinella and Regulus-regulus) matches long-term point-count data showing spatial segregation driven by habitat preferences rather than by temperature alone (Järvinen and Väisänen, 2006; Newton, 2003).

7 Discussion

We introduced mixed-mSSL to fit high-dimensional regression models with multiple, possibly dependent, binary and continuous outcomes. mixed-mSSL encourages sparsity through the use of element-wise spike-and-slab LASSO priors on the elements of the latent regression coefficient and

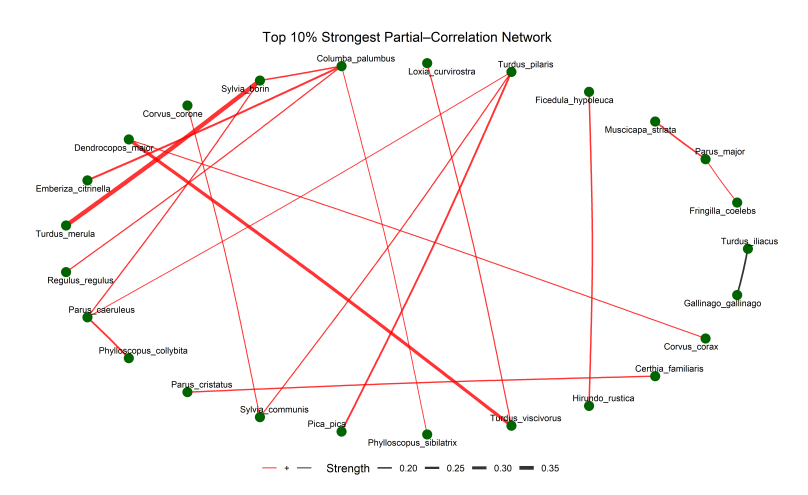


Figure 2: Covariate-adjusted partial-correlation network of bird species

residual precision matrices. We believe that mixed-mSSL offers a robust and practical solution for high-dimensional mixed-type datasets, balancing promising empirical performance with strong theoretical guarantees.

We developed a Monte Carlo Expectation-Conditional Maximization (MCECM) algorithm targeting the maximum a posteriori estimate of these parameters. Our algorithm is a natural extension of the ECM procedure proposed by Deshpande et al. (2019) to fit sparse multivariate linear regression models. On synthetic data mixed-mSSL outperformed another recently proposed Bayesian shrinkage method (Wang et al., 2025, mt-MBSP), which utilizes global-local shrinkage priors for the regression coefficients but cannot return a sparse latent precision matrix, in terms of support recovery, estimation, and prediction. When applied to the CKD dataset, mixed-mSSL identified more well-established biomarkers for CKD status and achieved smaller prediction error than mt-MBSP and separately modelling each outcome. mixed-mSSL also produced more accurate predictions with fewer selected covariates than mt-MBSP on the CRC microbiome data and uncovered a sparse residual dependence network among Finnish birds that is consistent with known co-occurrences.

Beyond demonstrating mixed-mSSL's excellent empirical performance, we derived the posterior contraction rates for the matrix of latent regression coefficients \boldsymbol{B} (Theorem 3) and the latent residual prediction matrix Ω (Theorem 6). While similar in spirit, our results substantially extend those proved in Wang et al. (2025) by (i) allowing the number of outcomes to diverge with n and (ii) showing that the posterior over Ω contracts. We further showed that with a natural truncation strategy, mixed-mSSL has the desirable sure screening property (Theorem 7), which guarantees that the truly non-zero entries in \boldsymbol{B} can be identified with high probability as n increases.

As alluded to in Section 2, we can easily extend mixed-mSSL to accommodate integer- or count-valued outcomes by using a different deterministic transformation. Practically, this requires changing the Monte Carlo E-step so that the missing latent components are drawn from multivariate normals whose entries are truncated to intervals like [a, a + 1] for some integer a, as opposed to half-spaces like $(-\infty, 0)$ or $(0, \infty)$. For such draws, we can still use LinESS. Analyzing such extensions theoretically introduces some new challenges, which can be overcome by developing bespoke tail bounds for interval-truncated normals and adapting our entropy calculations to handle shift-

ing truncation sets; we leave such exploration for future work. A more ambitious extension of mixed-mSSL would allow the transformation g to be learned from the data instead of being fixed a priori, similar to the STAR framework of Kowal and Canale (2020).

References

- Ash, R. B. and Doleans-Dade, C. A. (2000). Probability and Measure Theory. Elsevier Science.
- Bai, R. and Ghosh, M. (2018). High-dimensional multivariate posterior consistency under global-local shrinkage priors. *Journal of Multivariate Analysis*, 167:157–170.
- Banerjee, S. and Ghosal, S. (2015). Bayesian structure learning in graphical models. *Journal of Multivariate Analysis*, 136:147–162.
- Bhadra, A., Datta, J., Polson, N. G., and Willard, B. (2017). The Horseshoe+ estimator of ultrasparse signals. *Bayesian Analysis*, 12(4):1105 1131.
- Bradley, J. (2022). Joint Bayesian analysis of multiple response-types using the hierarchical generalized transformation model. *Bayesian Analysis*, 17(1):127–164.
- Canale, A. and Dunson, D. B. (2011). Bayesian kernel mixtures for counts. *Journal of the American Statistical Association*, 106(496):1528–1539.
- Canale, A. and Dunson, D. B. (2013). Nonparametric Bayes modelling of count processes. Biometrika, 100(4):801–816.
- Canale, A. and Dunson, D. B. (2014). Bayesian multivariate mixed-scale density estimation. arXiv: 1110.1265.
- Carvalho, C. M., Polson, N. G., and Scott, J. G. (2009). Handling sparsity via the horseshoe. In *Proceedings of the Twelfth International Conference on Artificial Intelligence and Statistics*.
- Castillo, I., Schmidt-Hieber, J., and van der Vaart, A. (2015). Bayesian linear regression with sparse priors. *The Annals of Statistics*, 43(5):1986–2018.
- Chen, X., Kang, X., Jin, R., and Deng, X. (2023). Bayesian sparse regression for mixed multi-responses with application to runtime metrics prediction in fog manufacturing. *Technometrics*, 65(2):206–219.
- Chib, S. and Greenberg, E. (1998). Analysis of multivariate probit models. *Biometrika*, 85:347–361.
- Deshpande, S. K., Ročková, V., and George, E. I. (2019). Simultaneous variable and covariance selection with the multivariate spike-and-slab lasso. *Journal of Computational and Graphical Statistics*, 28(4):921–931.
- Dunson, D. B. (2000). Bayesian latent variable models for clustered mixed outcomes. *Journal of the Royal Statistical Society Series B: Statistical Methodology*, 62(2):355–366.
- Ebiaredoh-Mienye, S. A., Swart, T. G., Esenogho, E., and Mienye, I. D. (2022). A machine learning method with filter-based feature selection for improved prediction of chronic kidney disease. *Bioengineering*, 9(8).

- Ekvall, K. O. and Molstad, A. J. (2022). Mixed-type multivariate response regression with covariance estimation. *Statistics in Medicine*, 41(15):2768–2785.
- Fan, J. and Lv, J. (2008). Sure independence screening for ultrahigh dimensional feature space. Journal of the Royal Statistical Society Series B: Statistical Methodology, 70(5):849–911.
- Feng, Q., Liang, S., Jia, H., Stadlmayr, A., Tang, L., Lan, Z., Zhang, D., Xia, H., Xu, X., Jie, Z., Su, L., Li, X., Li, X., Li, J., Xiao, L., Huber-Schönauer, U., Niederseer, D., Xu, X., Al-Aama, J. Y., Yang, H., Wang, J., Kristiansen, K., Arumugam, M., Tilg, H., Datz, C., and Wang, J. (2015). Gut microbiome development along the colorectal adenoma—carcinoma sequence. Nature Communications, 6(1):6528.
- Fitzmaurice, G. and Laird, N. (1997). Regression models for mixed discrete and continuous responses with potentially missing values. *Biometrics*, 53(1):110–122.
- Friedman, J. H., Hastie, T., and Tibshirani, R. (2010). Regularization paths for generalized linear models via coordinate descent. *Journal of Statistical Software*, 33(1):1–22.
- George, E. I. and McCulloch, R. E. (1993). Variable selection via Gibbs sampling. *Journal of the American Statistical Association*, 88(423):881–889.
- George, E. I. and Ročková, V. (2020). Comment: regularization via Bayesian penalty mixing. Technometrics, 62(4):438–442.
- Gessner, A., Kanjilal, O., and Hennig, P. (2020). Integrals over Gaussians under linear domain constraints. In *Proceedings of the Twenty Third International Conference on Artificial Intelligence and Statistics*.
- Ghosal, S. and van der Vaart, A. (2007). Convergence rates of posterior distributions for noniid observations. *Annals of Statistics*, 35(1):192–223.
- Hassanein, M. and Shafi, T. (2022). Assessment of glycemia in chronic kidney disease. *BMC Medicine*, 20(1):117.
- Hsieh, C.-J., Sustik, M. A., Dhillon, I. S., and Ravikumar, P. (2014). QUIC: Quadratic approximation for sparse inverse covariance estimation. *Journal of Machine Learning Research*, 15(83):2911–2947.
- Ishwaran, H. and Rao, J. S. (2005). Spike and slab variable selection: Frequentist and Bayesian strategies. *Annals of Statistics*, 33(2):730–773.
- Järvinen, O. and Väisänen, R. (2006). Changes in bird populations as criteria of environmental changes. *Ecography*, 2:75–80.
- Karlsson, F. H., Tremaroli, V., Nookaew, I., Bergström, G., Behre, C. J., Fagerberg, B., Nielsen, J., and Bäckhed, F. (2013). Gut metagenome in European women with normal, impaired and diabetic glucose control. *Nature*, 498(7452):99–103.
- Kostic, A. D., Chun, E., Robertson, L., Glickman, J. N., Gallini, C. A., Michaud, M., Clancy, T. E., Chung, D. C., Lochhead, P., Hold, G. L., El-Omar, E. M., Brenner, D., Fuchs, C. S., Meyerson, M., and Garrett, W. S. (2013). Fusobacterium nucleatum potentiates intestinal tumorigenesis and modulates the tumor-immune microenvironment. *Cell Host & Microbe*, 14(2):207–215.

- Kowal, D. R. and Canale, A. (2020). Simultaneous transformation and rounding (STAR) models for integer-valued data. *Electronic Journal of Statistics*, 14(1):1744–1772.
- Kumar, M., Dev, S., Khalid, M. U., Siddenthi, S., Noman, M., John, C., Akubuiro, C., Haider, A., Rani, R., Kashif, M., Varrassi, G., Khatri, M., Kumar, S., and Mohamad, T. (2023). The bidirectional link between diabetes and kidney disease: mechanisms and management. *Cureus*, 15:e45615.
- Laurent, B. and Massart, P. (2000). Adaptive estimation of a quadratic functional by model selection. *The Annals of Statistics*, 28(5):1302–1338.
- Li, X., Ghosh, J., and Villarini, G. (2023). A comparison of Bayesian multivariate versus univariate normal regression models for prediction. *The American Statistician*, 77(3):304–312.
- Lindström, Å., Green, M., Husby, M., Kålås, J. A., and Lehikoinen, A. (2015). Large-scale monitoring of waders on their Boreal and Arctic breeding grounds in Northern Europe. *Ardea*, 103(1):3–15.
- Liu, J., Huang, X., Chen, C., Wang, Z., Huang, Z., Qin, M., He, F., Tang, B., Long, C., Hu, H., Pan, S., Wu, J., and Tang, W. (2023). Identification of colorectal cancer progression-associated intestinal microbiome and predictive signature construction. *Journal of Translational Medicine*, 21(1):373.
- Louis, P., Hold, G. L., and Flint, H. J. (2014). The gut microbiota, bacterial metabolites and colorectal cancer. *Nature Reviews Microbiology*, 12(10):661–672.
- Mandic, M., Li, H., Safizadeh, F., Niedermaier, T., Hoffmeister, M., and Brenner, H. (2024). Correction: Is the association of overweight and obesity with colorectal cancer underestimated? An umbrella review of systematic reviews and meta-analyses. *European Journal of Epidemiology*, 39(2):231–231.
- McCulloch, C. (2008). Joint modelling of mixed outcome types using latent variables. *Statistical Methods in Medical Research*, 17(1):53–73. PMID: 17855745.
- Newton, I. (2003). Geographical patterns in bird migration. In Avian Migration, pages 211–224.
- Ovaskainen, O. and Abrego, N. (2020). *Joint Species Distribution Modelling: With Applications in R.* Cambridge University Press.
- Polson, N. G., Scott, J. G., and Winle, J. (2013). Bayesian inference for logistic models using Pólya-Gamma latent variables. *Journal of the American Statistical Association*, 108(504):1339–1349.
- Qin, J., Li, Y., Cai, Z., Shenghui, L., Zhu, J., Zhang, F., Liang, S., Zhang, W., Guan, Y., Shen, D., Peng, Y., Zhang, D., Jie, Z., Wu, W., Qin, Y., Xue, W., Li, J., Han, L., Lu, D., and Wang, J. (2012). A metagenome-wide association study of gut microbiota in type 2 diabetes. *Nature*, 490:55–60.
- Rasmussen, C. E. and Williams, C. K. I. (2005). Gaussian Processes for Machine Learning. The MIT Press.

- Razavi, S., Amirmozafari, N., Zahedi bialvaei, A., Navab-Moghadam, F., Khamseh, M. E., Alaei-Shahmiri, F., and Sedighi, M. (2024). Gut microbiota composition and Type 2 diabetes: Are these subjects linked together? *Heliyon*, 10(20):e39464.
- Ročková, V. and George, E. I. (2018). The spike-and-slab LASSO. *Journal of the American Statistical Association*, 113(521):431–444.
- Roverato, A. (2002). Hyper inverse wishart distribution for non-decomposable graphs and its application to Bayesian inference for gaussian graphical models. *Scandinavian Journal of Statistics*, 29(3):391–411.
- Sagar, K., Banerjee, S., Datta, J., and Bhadra, A. (2024). Precision matrix estimation under the horseshoe-like prior-penalty dual. *Electronic Journal of Statistics*, 18(1):1–46.
- Sarkar, P., Khare, K., and Ghosh, M. (2025). Posterior consistency in multi-response regression models with non-informative priors for the error covariance matrix in growing dimensions. Bernoulli, 31(3):2403–2433.
- Shen, Y. and Deshpande, S. K. (2022). Posterior contraction and uncertainty quantification for the multivariate spike-and-slab LASSO. [arXiv]:2209.04389.
- Shen, Y., Solís-Lemus, C., and Deshpande, S. K. (2024). Estimating sparse direct effects in multi-variate regression with the spike-and-slab lasso. *Bayesian Analysis*.
- Song, Q. and Liang, F. (2023). Nearly optimal Bayesian shrinkage for high dimensional regression. *Science China Mathematics*, 66(2):409–442.
- Virkkala, R. and Lehikoinen, A. (2014). Patterns of climate-induced density shifts of species: poleward shifts faster in northern Boreal birds than in southern birds. *Global Change Biology*, 20(10):2995–3003.
- Vogtmann, E., Hua, X., Zeller, G., Sunagawa, S., Voigt, A. Y., Hercog, R., Goedert, J. J., Shi, J., Bork, P., and Sinha, R. (2016). Colorectal cancer and the human gut microbiome: reproducibility with whole-genome shotgun sequencing. *PloS One*, 11(5):e0155362.
- Wagner, H. and Tüchler, R. (2010). Bayesian estimation of random effects models for multivariate responses of mixed data. *Computational Statistics & Data Analysis*, 54(5):1206–1218.
- Wang, S.-H., Bai, R., and Huang, H.-H. (2025). Two-step mixed-type multivariate Bayesian sparse variable selection with shrinkage priors. *Electronic Journal of Statistics*, 19(1):397–457.
- Watts, D. J. and Strogatz, S. H. (1998). Collective dynamics of 'small-world'networks. *Nature*, 393(6684):440–442.
- Wei, R. and Ghosal, S. (2020). Contraction properties of shrinkage priors in logistic regression. Journal of Statistical Planning and Inference, 207:215–229.
- Wirbel, J., Pyl, P. T., Kartal, E., Zych, K., Kashani, A., Milanese, A., Fleck, J. S., Voigt, A. Y., Palleja, A., Ponnudurai, R., et al. (2019). Meta-analysis of fecal metagenomes reveals global microbial signatures that are specific for colorectal cancer. *Nature Medicine*, 25:679–689.

- Yu, J., Feng, Q., Wong, S. H., Zhang, D., yi Liang, Q., Qin, Y., Tang, L., Zhao, H., Stenvang, J., Li, Y., et al. (2017). Metagenomic analysis of faecal microbiome as a tool towards targeted non-invasive biomarkers for colorectal cancer. *Gut*, 66(1):70–78.
- Zeller, G., Tap, J., Voigt, A. Y., Sunagawa, S., Kultima, J. R., Costea, P. I., Amiot, A., Böhm, J., Brunetti, F., Habermann, N., et al. (2014). Potential of fecal microbiota for early-stage detection of colorectal cancer. *Molecular Systems Biology*, 10(11):766.
- Zellner, A. (1962). An efficient method for estimating seemingly unrelated regressions and tests for aggregation bias. *Journal of the American Statistical Association*, 57(298):348–368.
- Zhang, R., Yao, Y., and Ghosh, M. (2022). Contraction of a quasi-Bayesian model with shrinkage priors in precision matrix estimation. *Journal of Statistical Planning and Inference*, 221:154–171.
- Zhou, Q., Yang, J., Vats, D., Roberts, G. O., and Rosenthal, J. S. (2022). Dimension-free mixing for high-dimensional Bayesian variable selection. *Journal of the Royal Statistical Society Series B: Statistical Methodology*, 84(5):1751–1784.
- Zito, A. and Miller, J. W. (2024). Compressive Bayesian non-negative matrix factorization for mutational signatures analysis. arXiv:2404.10964.

Supplementary Materials

A Proofs

We present the proofs of some of the theoretical results in this section.

A.1 Conditional posterior of the binary latents

We partition the precision matrix and latent mean as $\Omega = \begin{pmatrix} \Omega_{CC} & \Omega_{CB} \\ \Omega_{CB} & \Omega_{BB} \end{pmatrix}$, and $\boldsymbol{m}_i = \boldsymbol{B}^{\top} \boldsymbol{x}_i = \begin{pmatrix} \boldsymbol{m}_i^{(C)} \\ \boldsymbol{m}_i^{(B)} \end{pmatrix}$ respectively, where $\Omega_{BB} \in \mathbb{R}^{q_b \times q_b}$ and $\operatorname{diag}(\Omega_{BB}) = \mathbf{1}_{q_b}$. Following the multivariate Normal conditional distribution formula in Rasmussen and Williams (2005, Appendix A2), we have $\boldsymbol{z}_i^{(B)} | \boldsymbol{z}_i^{(C)} = \boldsymbol{y}_i^{(C)}, \boldsymbol{B}, \Omega \sim \mathcal{N}(\boldsymbol{m}_{B|C}, \Omega_{BB}^{-1})$ with $\boldsymbol{m}_{B|C} = \boldsymbol{m}_i^{(B)} - \Omega_{BB}^{-1}\Omega_{CB}(\boldsymbol{y}_i^{(C)} - \boldsymbol{m}_i^{(C)})$.

A.2 Correlation threshold for mixed-type outcomes

Suppose y_{i1} is continuous and y_{i2} is binary, with latent Gaussian variables $z_{i1} \sim \mathcal{N}(0,1)$, $z_{i2} \sim \mathcal{N}(0,1)$, and $Corr(z_{i1}, z_{i2}) = \rho$.

Then by Model 1, $y_{i1} = z_{i1}, y_{i2} = \mathbb{1}\{z_{i2} > 0\}$. We want $Corr(y_{i1}, y_{i2})$. Here, $Var(y_{i1}) = Var(z_{i1}) = 1$, $Var(y_{i2}) = Var(\mathbb{1}\{z_{i2} > 0\}) = \frac{1}{2}(1 - \frac{1}{2}) = \frac{1}{4}$. Following the ideas from Lemma 2.1 in Ekvall and Molstad (2022), for the numerator, $Cov(z_{i1}, \mathbf{1}\{z_{i2} > 0\})$, we write

$$\mathbb{E}\big[z_{i1} \, \mathbb{1}\{z_{i2} > 0\}\big] = \int_{-\infty}^{\infty} z_1 \, \mathbb{P}(z_{i2} > 0 \mid z_{i1} = z_1) \, \phi(z_1) \, \mathrm{d}z_1,$$

where $\phi(\cdot)$ is the standard normal pdf, and $\mathbb{P}\{z_{i2} > 0 \mid z_{i1} = z_1\} = \Phi\left(\rho z_1/\sqrt{1-\rho^2}\right)$. Therefore, $\operatorname{Cov}(z_{i1}, \mathbf{1}\{z_{i2} > 0\}) = \int_{-\infty}^{\infty} z_1 \, \phi(z_1) \, \Phi\left(\frac{\rho z_1}{\sqrt{1-\rho^2}}\right) dz_1$. Hence,

$$Corr(y_{i1}, y_{i2}) = \frac{\mathbb{E}[z_{i1} \, \mathbb{1}\{z_{i2} > 0\}]}{\frac{1}{2}} = 2 \int_{-\infty}^{\infty} z_1 \, \phi(z_1) \, \Phi\left(\frac{\rho \, z_1}{\sqrt{1 - \rho^2}}\right) dz_1.$$

As ρ increases toward 1, this integral grows but cannot exceed $\sqrt{\frac{2}{\pi}} \approx 0.8$. A rigorous argument uses dominated convergence to show $\lim_{\rho \to 1^-} \operatorname{Corr}(y_{i1}, y_{i2}) = \sqrt{\frac{2}{\pi}}$. To see this formally, we write $I_{\rho} = 2\int_{-\infty}^{\infty} z \,\phi(z) \,\Phi\left(\frac{\rho z}{\sqrt{1-\rho^2}}\right) dz$, $0 \le \rho < 1$, and define $h_{\rho}(z) = 2 \,z \,\phi(z) \,\Phi\left(\frac{\rho z}{\sqrt{1-\rho^2}}\right)$, $g(z) = 2 \,|z| \,\phi(z)$. For any fixed $z \ne 0$, $\frac{\rho z}{\sqrt{1-\rho^2}} \to \pm \infty$ as $\rho \uparrow 1$; hence $h_{\rho}(z) \to h(z) := 2 \,z \,\phi(z) \,\mathbf{1}_{\{z>0\}}$. Because $0 \le \Phi(\cdot) \le 1$, $0 \le h_{\rho}(z) \le g(z)$. Moreover, $\int_{-\infty}^{\infty} g(z) \,dz = \frac{4}{\sqrt{2\pi}} < \infty$, so g is integrable. Now, DCT gives

$$\lim_{\rho \uparrow 1} I_{\rho} \; = \; \int_{-\infty}^{\infty} h(z) \, dz \; = \; 2 \int_{0}^{\infty} z \, \phi(z) \, dz \; = \; 2 \, \frac{1}{\sqrt{2\pi}} \; = \; \sqrt{\frac{2}{\pi}}.$$

The same argument with $\rho \to -1^+$ gives the lower bound $-\sqrt{2/\pi}$.

Intuitively, $z_{i2} > 0$ only tracks the sign of z_{i2} , so it cannot fully capture the magnitude alignment of z_{i1} . This partial alignment caps the observed correlation below 1. Hence for a mixed continuous—binary pair, the observed correlation cannot exceed $\sqrt{2/\pi}$, reflecting a fundamental limit from thresholding one of the two latent variables. This completes the proof of the correlation bound in Lemma 1 for the mixed case.

A.3 Proof of Lemma 2

Proof. We write the row-wise decomposition

$$\|oldsymbol{B}_n - oldsymbol{B}_0\|_F^2 = \sum_{j=1}^{p_n} \|oldsymbol{b}_j^{(n)} - oldsymbol{b}_j^0\|_2^2 = \sum_{j \in S_0} \|oldsymbol{b}_j^{(n)} - oldsymbol{b}_j^0\|_2^2 + \sum_{j \notin S_0} \|oldsymbol{b}_j^{(n)}\|_2^2.$$

Hence,

$$\mathbb{P}\left(\|\boldsymbol{B}_{n}-\boldsymbol{B}_{0}\|_{F} < Cn^{-\frac{\rho}{2}}\epsilon_{n}\right) \geq \prod_{j \in S_{0}} \mathbb{P}\left(\|\boldsymbol{b}_{j}^{n}-\boldsymbol{b}_{j}^{0}\|_{2}^{2} < C^{2}\frac{\epsilon_{n}^{2}}{2s_{0}^{B}n^{\rho}}\right) \\
\times \mathbb{P}\left(\sum_{j \notin S_{0}} \|\boldsymbol{b}_{j}^{n}\|_{2}^{2} < C^{2}\frac{\epsilon_{n}^{2}}{2n^{\rho}}\right) \\
= \mathcal{A}_{1} \times \mathcal{A}_{2}$$

Define the two terms in the RHS as \mathcal{A}_1 and \mathcal{A}_2 respectively. Define $\Delta_n^2 = \frac{C^2 \epsilon_n^2}{2s_0^B n^\rho}$. Let us deal with \mathcal{A}_2 first. We have

$$\mathcal{A}_{2} = \mathbb{P}\left(\sum_{j \notin S_{0}} \|\boldsymbol{b}_{j}^{n}\|_{2}^{2} < s_{0}^{B} \Delta_{n}^{2}\right)$$

$$= 1 - \mathbb{E}\left[\mathbb{P}\left(\sum_{j \notin S_{0}} \|\boldsymbol{b}_{j}^{n}\|_{2}^{2} > s_{0}^{B} \Delta_{n}^{2} | \theta, \lambda_{0}, \lambda_{1}\right)\right]$$

$$\geq 1 - \mathbb{E}\left[\frac{\mathbb{E}(\sum_{j \notin S_{0}} \|\boldsymbol{b}_{j}^{n}\|_{2}^{2} | \theta, \lambda_{0}, \lambda_{1})}{s_{0}^{B} \Delta_{n}^{2}}\right]$$

$$= 1 - \frac{(p_{n} - s_{0}^{B})cn^{-(1+\rho)}/(p_{n}q_{n})}{s_{0}^{B} \Delta_{n}^{2}} \quad \text{(From Assumption (A6))}$$

$$\geq 1 - \frac{c}{C^{2}} \frac{n^{-(1+\rho)}}{q_{n}\epsilon_{n}^{2}}$$

$$\to 1 \text{ as } n \to \infty$$

The last line follows from Assumptions (A1) and (A2) implying $q_n \epsilon_n^2 \to \infty$. Thus there is a constant $D_0 > 0$ so that $A_2 \ge \exp(-D_0 n \epsilon_n^2)$.

Focusing on A_1 , we can write

$$\mathcal{A}_1 = \prod_{j \in S_0} \left[\int_{\|\boldsymbol{b}_j^n - \boldsymbol{b}_j^0\|_2^2 < \Delta_n^2} p(\boldsymbol{b}_j^n) d\boldsymbol{b}_j^n \right]$$

Breaking down this integral, we have

$$\mathcal{A}_{1} \geq \prod_{j \in S_{0}} \prod_{k=1}^{q_{n}} \int_{\left\{|b_{j,k}^{n} - b_{j,k}^{0}|^{2} < \frac{\Delta_{n}^{2}}{q_{n}}\right\}} \left[\left(\frac{1-\theta}{2}\right) \lambda_{0} \exp(-\lambda_{0}|b_{j,k}^{n}|) + \frac{\theta \lambda_{1}}{2} \exp(-\lambda_{1}|b_{j,k}^{n}|)\right] db_{j,k}^{n} \\
= \prod_{j \in S_{0}} \prod_{k=1}^{q_{n}} \int_{b_{j,k}^{0} - \frac{\Delta_{n}}{\sqrt{q_{n}}}}^{b_{j,k}^{0} + \frac{\Delta_{n}}{\sqrt{q_{n}}}} \left[\left(\frac{1-\theta}{2}\right) \lambda_{0} \exp(-\lambda_{0}|b_{j,k}^{n}|) + \frac{\theta \lambda_{1}}{2} \exp(-\lambda_{1}|b_{j,k}^{n}|)\right] db_{j,k}^{n} \\
\geq \prod_{j \in S_{0}} \prod_{k=1}^{q_{n}} \exp(-\lambda_{0}|b_{j,k}^{0}|) \int_{-\frac{\Delta_{n}}{\sqrt{q_{n}}}}^{\frac{\Delta_{n}}{\sqrt{q_{n}}}} \left(\frac{1-\theta}{2}\right) \lambda_{0} \exp(-\lambda_{0}|\Delta|) d\Delta \\
+ \prod_{j \in S_{0}} \prod_{k=1}^{q_{n}} \exp(-\lambda_{1}|b_{j,k}^{0}|) \int_{-\frac{\Delta_{n}}{\sqrt{q_{n}}}}^{\frac{\Delta_{n}}{\sqrt{q_{n}}}} \frac{\theta}{2} \lambda_{1} \exp(-\lambda_{1}|\Delta|) d\Delta$$

For $\Delta := \Delta_n / \sqrt{q_n}$ and using the inequality $1 - e^{-t} \ge t e^{-t}$, (t > 0) gives

$$1 - e^{-\lambda_j \Delta} \ge \lambda_j \Delta e^{-\lambda_j \Delta}, \quad j = 0, 1.$$

Hence for $f_{j,k}(t) = (1-\theta)\frac{\lambda_0}{2}e^{-\lambda_0|t|} + \theta\frac{\lambda_1}{2}e^{-\lambda_1|t|}$,

$$\int_{b_{j,k}^0 - \Delta}^{b_{j,k}^0 + \Delta} f_{j,k}(t) dt \ge \Delta \left[(1 - \theta) \lambda_0^2 e^{-\lambda_0(|b_{j,k}^0| + \Delta)} + \theta \lambda_1^2 e^{-\lambda_1(|b_{j,k}^0| + \Delta)} \right].$$

Assumption (A4) gives $|b_{j,k}^0| \leq a_1$. For sufficiently large $n, \Delta \leq 1$. Define

$$C_1 := e^{-(a_1+1)\min(\lambda_0,\lambda_1)} \lceil (1-\theta)\lambda_0^2 + \theta \lambda_1^2 \rceil > 0.$$

Then each univariate integral satisfies $\int_{b_{j,k}^0-\Delta}^{b_{j,k}^0+\Delta} f_{j,k}(t) dt \geq C_1 \Delta$. Since there are $s_0^B q_n$ coordinates in the active rows,

$$\mathcal{A}_{1} = \prod_{j \in S_{0}} \prod_{k=1}^{q_{n}} \int_{|t-b_{j,k}^{0}| < \Delta} f_{j,k}(t) dt \geq (C_{1}\Delta)^{s_{0}^{B}q_{n}} = (C_{1}\Delta_{n}/\sqrt{q_{n}})^{s_{0}^{B}q_{n}}.$$

Take logarithms and substitute $\Delta_n^2 = C^2 \epsilon_n^2/(2s_0^B n^{\rho})$:

$$\log A_1 \geq s_0^B q_n \left(\frac{1}{2} \log \Delta_n^2 - \frac{1}{2} \log q_n + \log C_1 \right) = -s_0^B q_n \left(\frac{1}{2} \log q_n - \frac{1}{2} \log \Delta_n^2 - \log C_1 \right).$$

Because $\epsilon_n^2 = \frac{\max(q_n, s_0^B) \log p_n}{n}$ and $\Delta_n^2 \approx \frac{\epsilon_n^2}{n^\rho}$,

$$s_0^B q_n \Big[\frac{1}{2} \log q_n - \frac{1}{2} \log \Delta_n^2 \Big] \le C_2 s_0^B q_n \Big(\log q_n + \log n^{\rho} - \log \epsilon_n^2 \Big) \le C_3 n \epsilon_n^2,$$

where the last inequality uses Assumptions (A1)–(A2): $s_0^B = o\left(n/\log p_n\right), \ q_n \leq n^b \ (b < \frac{1}{2}), \ \text{and} \log p_n \gg n^{-(1+\rho)} \max(s_0^B, q_n).$ Collecting constants, $\log \mathcal{A}_1 \geq -D_1 \, n \epsilon_n^2 \implies \mathcal{A}_1 \geq e^{-D_1 n \epsilon_n^2}, \ \text{as}$ required. Combining the two bounds for \mathcal{A}_1 and \mathcal{A}_2 with $D = D_0 + D_1$, we have $\mathbb{P}(\|\mathbf{B}_n - \mathbf{B}_0\|_F < Cn^{-\rho/2}\epsilon_n) \geq \mathcal{A}_1\mathcal{A}_2 \geq \exp(-Dn\epsilon_n^2).$

A.4 Proof of Lemma 4

As per the standard theory of posterior contraction established in Ghosal and van der Vaart (2007), we need to construct a sequence of sets (sieves) of bounded complexity that essentially "capture" the parameter space as $n \to \infty$. Then, we need to verify that the prior places enough mass (or concentration) around the true parameter within the sieves. The sieve construction for this problem is outlined as follows.

The sieve construction

We define $S \subset \mathcal{I} = \{1, \ldots, p_n\}$ be a set of row indices for the regression coefficients matrix. Let $S_0 \subset \{1, 2, \ldots, p_n\}$ denote the set of indices of the rows in \mathbf{B}_0 with at least one non-zero entry. Observe that $|S_0| = s_0^B \ge 1$ and $s_0^B = o(n)$. The sieve construction is similar to Wang et al. (2025). We define

$$\mathcal{M} = \{ S : S \supset S_0, S \neq S_0, |S| \le m_n \}$$

where m_n is a positive number satisfying $m_n \geq s_0^B$ and $m_n \log p_n = o(n\delta_n^2)$, where $\delta_n^2 = n^{-1} \{ \max(s_0^B, q_n) \times \log p_n \}$. For any set S, let $p^S = |S|$ and suppose \mathbf{B}^S and \mathbf{B}_0^S denote the $p^S \times q$ submatrices of \mathbf{B}_n and \mathbf{B}_0 containing the rows with indices in S. Similarly define \mathbf{x}^S as a $p^S \times 1$ sub-vector of \mathbf{x} which contains components with indices in S. For $\mathbf{B}^S \in \mathcal{M}$, consider the model:

$$z_i = (\boldsymbol{B}_0^S)' \boldsymbol{x}_i^S + \boldsymbol{\epsilon}_i, \quad i = 1, \dots, n$$

where $\epsilon_i \sim \mathcal{N}_q(\mathbf{0}, \Omega^{-1})$. The MLE for \mathbf{B}_0^S is $\hat{\mathbf{B}}^S$ where we know:

$$\operatorname{vec}(\hat{\boldsymbol{B}}^{S}) \sim \mathcal{N}_{p^{S}q} \left(\operatorname{vec}(\boldsymbol{B}_{0}^{S}), \left(\frac{1}{n} \sum_{i=1}^{n} \Omega \otimes (\boldsymbol{x}_{i}^{S}(\boldsymbol{x}_{i}^{S})') \right)^{-1} \right)$$
(A1)

Finally, the sieve is defined by the collection-

$$C_n = \bigcup_{S \in \mathcal{M}} \left\{ \|\hat{\boldsymbol{B}}^S - \boldsymbol{B}_0^S\|_F > \frac{\epsilon \delta_n}{2} \right\}$$
 (A2)

Corollary: Following the arguments in Wang et al. (2025) that for any prior $p(\mathbf{B}_n)$ satisfying the inequality in Lemma 2 and the test function $\Phi_n = \mathbb{1}(\mathbf{Z}_n \in \mathcal{C}_n)$, where \mathcal{C}_n is the same sieve as in Equation A2, we have:

(1)
$$\mathbb{E}_{\boldsymbol{B}_0}(\Phi_n) \le \exp\left(-\frac{Cn\delta_n^2}{2}\right)$$

(2)
$$\sup_{\boldsymbol{B}_n \in \mathcal{B}_{\epsilon}} \mathbb{E}_{\boldsymbol{B}_n} (1 - \Phi_n) \le \exp(-Cn\delta_n^2)$$

where we call $\mathcal{B}_{\epsilon} = \{ \mathbf{B}_n : \|\mathbf{B}_n - \mathbf{B}_0\|_F > \epsilon \delta_n \}.$

(1) Type-I error bound. Writing down the score equations of the Gaussian likelihood in $\mathbf{A1}$, we have $\operatorname{vec}(\hat{\mathbf{B}}^S) = \operatorname{vec}(\mathbf{B}_0^S) + \mathbf{V}_S^{-1} g_S$, where $g_S = \frac{1}{n} \sum_{i=1}^n (\Omega \mathbf{x}_i^S) \otimes \mathbf{z}_i$, and $\mathbf{V}_S = \left(\frac{1}{n} \sum_{i=1}^n \Omega \otimes (\mathbf{x}_i^S(\mathbf{x}_i^S)')\right)$. Now, under $\mathbf{B} = \mathbf{B}_0$, we have $\operatorname{vec}(\hat{\mathbf{B}}^S - \mathbf{B}_0^S) \sim \mathcal{N}_{p^S q_n}(\mathbf{0}, \mathbf{V}_S^{-1})$. Assumptions (A3) and (A5) imply there exist constants $0 < c_{\star} \leq C_{\star} < \infty$ independent of n, S such that $c_{\star} p^S q_n / n \mathbf{I}_{p^S q_n} \lesssim \mathbf{V}_S^{-1} \lesssim C_{\star} p^S q_n / n \mathbf{I}_{p^S q_n}$. Combining these two results, we have

$$T_S = \|\hat{\boldsymbol{B}}^S - \boldsymbol{B}_0^S\|_F^2 = \|\boldsymbol{V}_S^{1/2} \boldsymbol{u}\|_2^2, \ \boldsymbol{u} \sim \mathcal{N}_{p^S q_n}(\boldsymbol{0}, \boldsymbol{I}_{p^S q_n}).$$

Hence, it is worthwhile to observe that $c_{\star}p^{S}q/n\chi_{p^{S}q}^{2} \leq T_{S} \leq C_{\star}p^{S}q/n\chi_{p^{S}q}^{2}$. This leads to

$$\mathbb{P}_{\boldsymbol{B}_0}\left(T_S > \frac{1}{4}\epsilon^2 \delta_n^2\right) \le \mathbb{P}\left(\chi_{p^S q}^2 > \frac{1}{4} \frac{n\epsilon^2 \delta_n^2}{C_{\star} p^S q}\right).$$

Applying a χ^2 tail inequality inspired from Lemma 1 of Laurent and Massart (2000), we have for $R \sim \chi_d^2$, then $\mathbb{P}(R-d>2\sqrt{dx}+2x) \leq \exp(-x)$. We plug in $d=p^Sq_n$ and choose $x=\frac{n\epsilon^2\delta_n^2}{8C_\star}$. Since $p^Sq_n \leq m_nq_n = O(\max\{q_n,s_0^B\})$, assumption (A1) implies $x\gg p^Sq_n$ for large n. Then $2\sqrt{p^Sq_nx}+2x\leq \frac{n\epsilon^2\delta_n^2}{8C_\star}$, so taking $c=\epsilon^2/(8C_\star)$, we have

$$\mathbb{P}_{\boldsymbol{B}_0}\left(T_S > \frac{1}{4}\epsilon^2 \delta_n^2\right) \le \exp\{-cn\delta_n^2\}. \tag{A3}$$

Now, for any $k > s_0^B$ we use the standard entropy bound $\binom{p_n}{k} \leq (ep_n/k)^k$. Therefore

$$|\mathcal{M}| = \sum_{k=s_0^B+1}^{m_n} \binom{p_n}{k} \le \sum_{k=s_0^B+1}^{m_n} \left(\frac{ep_n}{k}\right)^k \le m_n \left(\frac{ep_n}{m_n}\right)^{m_n}. \tag{A4}$$

Because $m_n \log p_n = o(n\delta_n^2)$, $\log |\mathcal{M}| = O(m_n \log p_n) = o(n\delta_n^2)$. Using the sieve definition and the union bound we have:

$$\mathbb{E}_{\boldsymbol{B}_0}[\Phi_n] = \mathbb{P}_{\boldsymbol{B}_0}(\boldsymbol{Z}_n \in \mathcal{C}_n)$$

$$\leq \sum_{S \in \mathcal{M}} \mathbb{P}_{\boldsymbol{B}_0} \left(T_S > \frac{1}{4} \epsilon^2 \delta_n^2 \right)$$

$$\leq |\mathcal{M}| \exp(-cn\delta_n^2)$$

$$\leq \exp\left\{ -\frac{1}{2} cn\delta_n^2 \right\}.$$

Setting C = c/2, establishes the required bound $\mathbb{E}_{B_0}[\Phi_n] \leq \exp(-Cn\delta_n^2)$.

(2) Type-II error bound. Let $\mathbf{B}_n \in \mathcal{B}_{\epsilon}$. Set $S^* = S_0 \cup \{j : \mathbf{b}_j^{(n)} \neq \mathbf{b}_j^0\}$. Then $S^* \supset S_0$ and $|S^*| \leq s_0^B + d \leq m_n$ with

$$d = \left| \left\{ j : \boldsymbol{b}_{j}^{(n)} \neq \boldsymbol{b}_{j}^{0} \right\} \right| \leq \frac{\|\boldsymbol{B}_{n} - \boldsymbol{B}_{0}\|_{F}^{2}}{\Delta_{n}^{2}}, \quad \Delta_{n}^{2} = \frac{C^{2} \epsilon_{n}^{2}}{2s_{0}^{B} n^{\rho}}.$$

Thus $S^* \in \mathcal{M}$. Using the triangle inequality,

$$\|\hat{B}^{S^{\star}} - B_0^{S^{\star}}\|_F \ge \|B_n^{S^{\star}} - B_0^{S^{\star}}\|_F - \|\hat{B}^{S^{\star}} - B_n^{S^{\star}}\|_F.$$

Because $\|\boldsymbol{B}_n - \boldsymbol{B}_0\|_F > \epsilon \delta_n$ and S^* contains all rows that differ, the first term on the RHS exceeds $\epsilon \delta_n$; hence

$$\left\{ \boldsymbol{Z}_{n} \notin \mathcal{C}_{n} \right\} \subseteq \left\{ \forall S \in \mathcal{M} : \| \widehat{\boldsymbol{B}}^{S} - \boldsymbol{B}_{n}^{S} \|_{F} \leq \frac{1}{2} \epsilon \delta_{n} \right\}.$$
 (A5)

Applying A3 inside A5 and summing,

$$P_{\boldsymbol{B}_n}(1-\Phi_n) \leq \sum_{S\in\mathcal{M}} \exp\left\{-c\,n\delta_n^2\right\} = |\mathcal{M}| \exp\left\{-c\,n\delta_n^2\right\}.$$

Because $|\mathcal{M}| \leq \sum_{k=s_0^B+1}^{m_n} {p_n \choose k} \leq \exp\{m_n \log(p_n e/m_n)\}$ and $m_n \log p_n = o(n\delta_n^2)$ by construction, $\log |\mathcal{M}| = o(n\delta_n^2)$. Hence for some C > 0 independent of n,

$$\sup_{\boldsymbol{B}_n \in \mathcal{B}_{\epsilon}} P_{\boldsymbol{B}_n} (1 - \Phi_n) \leq \exp\left\{ -C \, n \delta_n^2 \right\},\,$$

completing the proof.

Thus, we only need to prove the following proposition to complete the proof of Lemma 4.

Proposition A1. Under the assumptions (A1)-(A6), for the SSL prior $p(\mathbf{B}_n)$ satisfying Lemma 2, we have that for any arbitrary $\epsilon > 0$ and $\epsilon_n^2 = n^{-1} \{ \max(s_0^B, q_n) \times \log p_n \}$,

$$\sup_{\boldsymbol{B}_0} \mathbb{E}_{\boldsymbol{B}_0} \mathbb{P} (\|\boldsymbol{B}_n - \boldsymbol{B}_0\|_F > \delta \epsilon_n | \boldsymbol{Z}_n) \to 0$$

as $n \to \infty$.

Proof. The proof follows the lines of Wang et al. (2025) and Bai and Ghosh (2018). We define the test function $\Phi_n = \mathbb{1}(\mathbf{Z}_n \in \mathcal{C}_n)$ and the Frobenius neighborhood $\mathcal{B}_{\delta} = \{\|\mathbf{B}_n - \mathbf{B}_0\|_F > \delta \epsilon_n\}$.

Let us consider the two integrals

$$J_{\mathcal{B}_{\delta}} = \int_{\boldsymbol{B}_{n} \in \mathcal{B}_{\delta}} \frac{p(\boldsymbol{Z}_{n}|\boldsymbol{B}_{n})}{p(\boldsymbol{Z}_{n}|\boldsymbol{B}_{0})dP(\boldsymbol{B}_{n})} \text{ and } J_{n} = \int \frac{p(\boldsymbol{Z}_{n}|\boldsymbol{B}_{n})}{p(\boldsymbol{Z}_{n}|\boldsymbol{B}_{0})}dP(\boldsymbol{B}_{n})$$

It is well-known that the posterior probability $\mathbb{P}(\mathcal{B}_{\delta}|\mathbf{Z}_n)$ can be expressed as

$$\mathbb{P}(\mathcal{B}_{\delta}|\mathbf{Z}_n) = \frac{J_{\mathcal{B}_{\delta}}}{J_n} \leq \Phi_n + (1 - \Phi_n) \frac{J_{\mathcal{B}_{\delta}}}{J_n}$$

By Markov's inequality and the corollary above, we have

$$\mathbb{P}\left(\Phi_n \ge \exp\left(\frac{-Cn\epsilon_n^2}{4}\right)\right) \le \exp\left(\frac{-Cn\epsilon_n^2}{4}\right)$$

Using the Borel-Cantelli lemma, we can deduce that $\mathbb{P}\left(\Phi_n \geq \exp\left(\frac{-Cn\epsilon_n^2}{4}\right)\right)$ infinitely often = 0, which implies that $\Phi_n \to 0$ a.s. in $\mathbb{P}_{\boldsymbol{B}_0}$ as $n \to \infty$.

Similarly, we can say that

$$\mathbb{E}_{\boldsymbol{B}_0}[(1-\Phi_n)J_{\mathcal{B}_{\delta}}] \leq \mathbb{P}(\boldsymbol{B}_n \in \mathcal{B}_{\delta}) \sup_{\boldsymbol{B}_n \in \mathcal{B}_{\delta}} \mathbb{E}_{\boldsymbol{B}_0}(1-\Phi_n)$$
$$\leq \exp(-Cn\epsilon_n^2)$$

Again by Borel-Cantelli, we can argue that $(1 - \Phi_n)J_{\mathcal{B}_{\delta}} \to 0$ a.s. in $\mathbb{P}_{\mathbf{B}_0}$ as $n \to \infty$.

Finally, we need to show that $\exp\left(\frac{Cn\epsilon_n^2}{2}\right)J_n\to\infty$ a.s. in $\mathbb{P}_{\boldsymbol{B}_0}$ as $n\to\infty$. See that

$$\log \frac{p(\boldsymbol{Z}_n|\boldsymbol{B}_n)}{p(\boldsymbol{Z}_n|\boldsymbol{B}_0)} = -\frac{1}{2} \sum_{i=1}^n [(\boldsymbol{z}_i - \boldsymbol{B}_n' \boldsymbol{x}_i)' \Omega(\boldsymbol{z}_i - \boldsymbol{B}_n' \boldsymbol{x}_i) \\ - (\boldsymbol{z}_i - \boldsymbol{B}_0' \boldsymbol{x}_i)' \Omega(\boldsymbol{z}_i - \boldsymbol{B}_0' \boldsymbol{x}_i)] \\ \leq \frac{1}{2} \sum_{i=1}^n \operatorname{tr} [\Omega(\boldsymbol{B}_n' \boldsymbol{x}_i - \boldsymbol{B}_0' \boldsymbol{x}_i) (\boldsymbol{B}_n' \boldsymbol{x}_i - \boldsymbol{B}_0' \boldsymbol{x}_i)'] \\ + \sum_{i=1}^n [\operatorname{tr} (\Omega(\boldsymbol{B}_n' \boldsymbol{x}_i - \boldsymbol{B}_0 \boldsymbol{x}_i) (\boldsymbol{B}_n' \boldsymbol{x}_i - \boldsymbol{B}_0 \boldsymbol{x}_i)'] \\ \times \operatorname{tr} [\Omega(\boldsymbol{z}_i - \boldsymbol{B}_0 \boldsymbol{x}_i) (\boldsymbol{z}_i - \boldsymbol{B}_0 \boldsymbol{x}_i)']^{\frac{1}{2}}$$

Based on Wang et al. (2025)'s proof, we can define $\mathcal{D}_n = \left\{ \boldsymbol{B}_n : \log \frac{p(\boldsymbol{Z}_n | \boldsymbol{B}_n)}{p(\boldsymbol{Z}_n | \boldsymbol{B}_0)} < n\epsilon_n^2 v \right\}$ for $0 < v < \frac{C}{2}$. Thus, from the previous inequality and the fact that

$$\mathbb{P}\left(\left\{\operatorname{tr}\sum_{i=1}^{n}\Omega(\boldsymbol{z}_{i}-\boldsymbol{B}_{0}'\boldsymbol{x}_{i})(\boldsymbol{z}_{i}-\boldsymbol{B}_{0}'\boldsymbol{x}_{i})'\right\}>n^{1+\rho}\text{ i.o.}\right)=0,$$

we can conclude that

$$\mathbb{P}(\mathcal{D}_n|\mathbf{Z}_n) \ge \mathbb{P}\left(\frac{1}{n\epsilon_n^2} \left\{ \operatorname{tr} \sum_{i=1}^n \Omega(\mathbf{B}_n'\mathbf{x}_i - \mathbf{B}_0'\mathbf{x}_i)(\mathbf{B}_n'\mathbf{x}_i - \mathbf{B}_0'\mathbf{x}_i)' \right\} < \frac{Cv^2}{n^{1+\rho}} \right)$$

$$\ge \mathbb{P}\left(\|\mathbf{B}_n - \mathbf{B}_0\|_F < \frac{Cv\epsilon_n}{\lambda_1 n^{\frac{\rho}{2}}} \right)$$

$$\ge \exp(-Dn\epsilon_n^2)$$

where $D \in (0, C/2 - v)$.

The final ingredient of the proof recipe for Theorem 3 is by proving Lemma 5, showing that the effective support of \mathbb{Z}_n is \mathbb{Z}_n .

Proof of Lemma 5. We treat continuous and binary responses separately. For every continuous coordinate, the model enforces $z_{ik} = y_{ik}$ deterministically. Because each y_{ik} is assumed to be sub-Gaussian (Assumptions (A3)-(A4)), the diagonal sub-Gaussian tail bound gives $\Pr(|y_{ik}| > M_0) \le 2 \exp\{-M_0^2/2\sigma_{\max}^2\}$, where $\sigma_{\max}^2 < \infty$ is an upper bound on the conditional variance. Choosing $M_0 \ge 4\sigma_{\max}\sqrt{\log n}$ makes this probability at most $2n^{-8}$. A union bound over at most $nq_c \le n^{3/2}$ indices (Assumption (A1): $q_c \le q_n \le n^b$ with b < 1/2) shows that

$$\mathbb{P}\left(\exists (i, k \le q_c) : |z_{ik}| > M_0\right) \le 2n^{-5},$$

so the continuous part already satisfies the desired bound. Conditional on \mathbf{Y}_n , \mathbf{X}_n and the parameters, each latent z_{ik} $(k > q_c)$ is a univariate truncated normal, standard Mills–ratio bounds for a truncated normal imply that for any t > 0, $\mathbb{P}\left(|z_{ik} - \theta_{ik}| > t \mid \mathbf{Y}_n\right) \leq 2e^{-t^2/2}$. Set $t = C_0\sqrt{\log n}$. Then

$$\mathbb{P}\left(|z_{ik} - \theta_{ik}| > C_0 \sqrt{\log n} \mid Y_n\right) \leq 2n^{-C_0^2/2}.$$

Choose C_0 so that $c := C_0^2/2 > 2$. With this choice $2n^{-c} \le 2n^{-2}$. There are $nq_b \le nq_n \le n^{1+b}$ binary latents. By the union bound,

$$\mathbb{P}\left(\exists (i, k > q_c) : |z_{ik} - \theta_{ik}| > C_0 \sqrt{\log n} \, | \, \mathbf{Y}_n\right) \leq 2n^{-c} \left(nq_n\right) \leq 2n^{-c+b+1}$$

Since c > 2 and $b < \frac{1}{2}$, the exponent -c + b + 1 < -1; hence the right-hand side is $o(n^{-1})$. Define $\delta_n := 2n^{-5} + 2n^{-c+b+1}$, which satisfies $\delta_n \to 0$. Combining the two parts, $\mathbb{P}\left(\mathbf{Z}_n \notin \mathcal{Z}_n \mid \mathbf{Y}_n\right) \leq \delta_n$ for all sufficiently large n. This proves the lemma.

A.5 Proof of Theorem 3

Combining all the previous lemmas, we now present the proof of Theorem 3:

Proof. By Lemma 4 (the conditional version), we know that for any $(\mathbf{Y}_n, \mathbf{Z}_n)$ in the good set \mathcal{Z}_n , the posterior mass outside $\{\|\mathbf{B}_n - \mathbf{B}_0\|_F \leq M \epsilon_n\}$ is at most some small δ'_n . On the complement \mathcal{Z}_n^c , we do not control that posterior mass, but from Lemma 5 we know $\mathbb{P}(\mathbf{Z}_n \notin \mathcal{Z}_n \mid \mathbf{Y}_n) \leq \delta_n$.

Hence, unconditionally,

$$\mathbb{P}(\|\boldsymbol{B}_{n} - \boldsymbol{B}_{0}\|_{F} > M \, \epsilon_{n} \mid \boldsymbol{Y}_{n}) = \int \mathbb{P}(\|\boldsymbol{B}_{n} - \boldsymbol{B}_{0}\|_{F} > M \, \epsilon_{n} \mid \boldsymbol{Y}_{n}, \boldsymbol{Z}_{n}) \, \mathbb{P}(\boldsymbol{Z}_{n} \mid \boldsymbol{Y}_{n}) \, d\boldsymbol{Z}_{n} \\
\leq \int_{\mathcal{Z}_{n}} \delta'_{n} \, \mathbb{P}(\boldsymbol{Z}_{n} \mid \boldsymbol{Y}_{n}) \, d\boldsymbol{Z}_{n} + \int_{\mathcal{Z}_{n}^{c}} 1 \times \mathbb{P}(\boldsymbol{Z}_{n} \mid \boldsymbol{Y}_{n}) \, d\boldsymbol{Z}_{n} \\
\leq \delta'_{n} + \delta_{n}.$$

Because $\delta'_n \to 0$ and $\delta_n \to 0$ as $n \to \infty$, it follows that

$$\mathbb{P}(\|\boldsymbol{B}_n - \boldsymbol{B}_0\|_F > M \epsilon_n \mid \boldsymbol{Y}_n) \longrightarrow 0.$$

Finally, taking the supremum over B_0 and the expectation $\mathbb{E}_{B_0}[\cdots]$ does not alter this limiting behavior, giving

$$\sup_{\boldsymbol{B}_0} \mathbb{E}_{\boldsymbol{B}_0} \Big[\mathbb{P} \Big(\|\boldsymbol{B}_n - \boldsymbol{B}_0\|_F > M \, \epsilon_n \, \Big| \, \boldsymbol{Y}_n \Big) \Big] \, \to \, 0.$$

This completes the proof.

A.6 Proof of Theorem 6

The key to this proof lies in proving the following lemma.

Lemma A2 (Conditional posterior contraction for Ω). Under the SSL prior configuration $p(\Omega)$ the posterior distribution of Ω satisfies for a sufficiently large M > 0,

$$\sup_{\Omega_0} \mathbb{E}_{\Omega_0} \left[\mathbb{P} \left(\|\Omega - \Omega_0\|_F > M \tilde{\epsilon}_n | \boldsymbol{Y}_n, \boldsymbol{Z}_n \right) \right] \longrightarrow 0$$

Proof. Since we are interested in the marginal posterior contraction of Ω to the true precision matrix Ω_0 , we can consider the matrix of regression coefficients \boldsymbol{B} to be fixed. WLOG, we can assume that $\boldsymbol{Z}_n = (\boldsymbol{z}_1, ..., \boldsymbol{z}_n)'$ is a random sample from a q-dimensional Normal distribution with mean $\boldsymbol{0}$ and a covariance matrix Ω_0^{-1} , where $\Omega_0 \in \mathcal{U}(k_1, s_0^{\Omega})$.

Proposition A3. Under the assumptions (B1),(B2) and (A5) considering the SSL prior configuration, the posterior distribution of Ω satisfies

$$\mathbb{E}_0\left[\mathbb{P}\{\|\Omega - \Omega_0\|_F > M\tilde{\epsilon}_n | \mathbf{Z}_n\}\right] \to 0$$

for $\tilde{\epsilon}_n^2 = n^{-1}\{(q_n + s_0^{\Omega}) \times \log q_n\}$ and a sufficiently large M > 0.

Proof. The proof of the above proposition follows the trajectory of showing that

- (i) The prior concentration rate of the KL $\tilde{\epsilon}_n^2$ neighborhoods is at least $\exp(-cn\tilde{\epsilon}_n^2)$.
- (ii) For a suitably chosen sieve of densities \mathcal{P}_n , its metric entropy is bounded by $Cn\tilde{\epsilon}_n^2$ for a constant C > 0.
- (iii) $\Pi(\mathcal{P}_n^c) \leq \exp(-c'n\tilde{\epsilon}_n^2)$ for a constant c' > 0.

(i) Prior concentration

Suppose $d_1, ..., d_p$ denote the eigen values of $\Omega_0^{-\frac{1}{2}}\Omega\Omega_0^{-\frac{1}{2}}$. Then according to the Lemma S.3.1 in Sagar et al. (2024), we have:

$$K(p_{\Omega_0}, p_{\Omega}) = \int p_{\Omega_0} \log \left(\frac{p_{\Omega_0}}{p_{\Omega}} \right) = -\frac{1}{2} \sum_{i=1}^n (\log d_i + (1 - d_i)),$$

$$V(p_{\Omega_0}, p_{\Omega}) = \int p_{\Omega_0} \log^2 \left(\frac{p_{\Omega_0}}{p_{\Omega}} \right) = -\frac{1}{2} \sum_{i=1}^n (1 - d_i)^2 + K(p_{\Omega_0}, p_{\Omega})^2.$$

It can be shown that both $K(p_{\Omega_0}, p_{\Omega}) \lesssim \sum_{i=1}^n (1-d_i)^2$ and $V(p_{\Omega_0}, p_{\Omega}) \lesssim \sum_{i=1}^n (1-d_i)^2$. But, it is worthwhile to note that

$$\sum_{i=1}^{n} (1 - d_i)^2 = \|\Omega_0^{-\frac{1}{2}} (\Omega - \Omega_0) \Omega_0^{-\frac{1}{2}}\|_2^2 \le \frac{1}{k_1^2} \|\Omega - \Omega_0\|_2^2$$

Hence, we have for a sufficiently small constant $c_1 > 0$,

$$\Pi(\mathcal{B}(p_0, \tilde{\epsilon}_n)) \ge \Pi\{\||\Omega - \Omega_0\|_2 \le c_1 \tilde{\epsilon}_n\} \ge \Pi\left\{\|\Omega - \Omega_0\|_{\infty} \le \frac{c_1 \tilde{\epsilon}_n}{q_n}\right\}$$

The rightmost term can be asymptotically bounded below using

$$\begin{split} \Pi\left\{\|\Omega-\Omega_0\|_{\infty} &\leq \frac{c_1\tilde{\epsilon}_n}{q_n}\right\} \gtrsim \left(\frac{c_1\tilde{\epsilon}_n}{q_n}\right)^{q_n+s_0^{\Omega}} \prod_{\{\omega_{ij,0}=0\}} \pi\left(|\omega_{ij}| \leq \frac{c_1\tilde{\epsilon}_n}{q_n}\right) \\ &\geq (1-\eta)^{Q-s_0^{\Omega}} \left(\frac{c_1\tilde{\epsilon}_n}{q_n}\right)^{q_n+s_0^{\Omega}} \prod_{i,j\in(S_0^{\Omega})^c} \int_{|\omega_{ij}| \leq \frac{c_1\tilde{\epsilon}_n}{q_n(Q-s_0^{\Omega})}} \frac{\xi_0}{2} \exp(-\xi_0|\omega_{ij}|) d\omega_{ij} \\ &\geq (1-\eta)^{Q-s_0^{\Omega}} \left(\frac{c_1\tilde{\epsilon}_n}{q_n}\right)^{q_n+s_0^{\Omega}} \prod_{i,j\in(S_0^{\Omega})^c} \left[1 - \frac{q_n(Q-s_0^{\Omega})}{c_1\tilde{\epsilon}_n} \mathbb{E}_{\pi}|\omega_{ij}|\right] \\ &= (1-\eta)^{Q-s_0^{\Omega}} \left(\frac{c_1\tilde{\epsilon}_n}{q_n}\right)^{q_n+s_0^{\Omega}} \left[1 - \frac{q_n(Q-s_0^{\Omega})}{c_1\tilde{\epsilon}_n\xi_0}\right]^{Q-s_0^{\Omega}} \\ &\gtrsim (1-\eta)^{Q-s_0^{\Omega}} \left(\frac{c_1\tilde{\epsilon}_n}{q_n}\right)^{q_n+s_0^{\Omega}} \left[1 - \frac{1}{Q-s_0^{\Omega}}\right]^{Q-s_0^{\Omega}} \\ &\approx (1-\eta)^{Q-s_0^{\Omega}} \left(\frac{c_1\tilde{\epsilon}_n}{q_n}\right)^{q_n+s_0^{\Omega}} \end{split}$$

where $Q = \frac{q_n(q_n-1)}{2}$ and S_0^{Ω} is the set of non-zero free parameters in Ω . It is evident from the assumption (B2) and the fact that $Q - s_0^{\Omega} \to \infty$, that $(1-\eta)^{Q-s_0^{\Omega}} \geq \left(1 - \frac{1}{q_n^a}\right)^{Q-s_0^{\Omega}} \to 1$. The inequality asymptotically becomes:

$$\Pi\left\{\|\Omega - \Omega_0\|_{\infty} \le \frac{c_1\tilde{\epsilon}_n}{q_n}\right\} \gtrsim \left(\frac{c_1\tilde{\epsilon}_n}{q_n}\right)^{q_n + s_0^{\Omega}}$$

. We have the exact rate $\tilde{\epsilon}_n$ by equating the prior concentration rate condition given by

$$(q_n + s_0^{\Omega}) \left(\log q_n + \log \left(\frac{1}{\tilde{\epsilon}_n} \right) \right) \simeq n\tilde{\epsilon}_n^2$$

This yields $\tilde{\epsilon}_n = \sqrt{\frac{(q_n + s_0^{\Omega}) \log q_n}{n}}$.

(ii) Sieve Construction and complexity

We consider the sieve similar to Sagar et al. (2024). It is given by

$$\mathcal{P}_n = \{ \Omega \in \mathcal{M}_q^+(\lambda) : \sum_{j,k} \mathbb{1}(|\omega_{jk}| > \nu_n) \le r_n, \|\Omega\|_{\infty} \le B \}$$

Here $\nu_n = \tilde{\epsilon}_n/q_n^b$ for b > 0, and a large enough B > 0. We can calculate the covering number N using the combinatorial argument that since all the elements in Ω are less than B in absolute value and the maximum number of elements of Ω exceeding ν_n is at most r_n ,

$$N = \sum_{j=1}^{r_n} \left(\frac{Bq_n^b}{\tilde{\epsilon}_n} \right)^{q_n + j} \begin{pmatrix} \binom{q_n}{2} \\ j \end{pmatrix}$$

The $\tilde{\epsilon}_n/q_n^b$ -metric entropy w.r.t. the L_{∞} norm is given by $\log N$. See that,

$$\log N = \log \left\{ \left(\frac{Bq_n^b}{\tilde{\epsilon}_n} \right)^{q_n} \right\} + \log \left\{ \sum_{j=1}^{r_n} \left(\frac{Bq_n^b}{\tilde{\epsilon}_n} \right)^j \binom{q_n}{2} \right\}$$

$$\leq \log \left\{ \left(\frac{Bq_n^b}{\tilde{\epsilon}_n} \right)^{q_n} \right\} + \log \left\{ r_n \left(\frac{Bq_n^b}{\tilde{\epsilon}_n} \right)^{r_n} \binom{q_n + \binom{q_n}{2}}{j} \right) \right\}$$

$$\lesssim (r_n + q_n) \left(\log q_n + \log B + \log \left(\frac{1}{\tilde{\epsilon}_n} \right) \right)$$

If we choose $r_n \sim \frac{c_1 n \tilde{\epsilon}_n^2}{\log n}$ and $B \sim c_2 n \tilde{\epsilon}_n^2$ for $c_1, c_2 > 0$, then we have $\log N \leq \tilde{C} n \tilde{\epsilon}_n^2$ for a constant $\tilde{C} > 0$.

(iii) Complement sieve probability

It is well known from Shen and Deshpande (2022) and Sagar et al. (2024) that

$$\Pi(\mathcal{P}_n^c) \leq \Pi(N \geq r_n + 1) + \Pi(\|\Omega\|_{\infty} > B)$$

The first term in the RHS can be bounded using the results on bounding the Binomial CDF in Song and Liang (2023) and Sagar et al. (2024). We consider the prior on the unconstrained Ω as Π^* . Using the fact from the proof of prior concentration, we know that $P(|\omega_{ij}| > \nu_n) \leq \frac{1}{q_n^a}$, we can infer that

$$\Pi^*(N \geq r_n + 1) \leq \exp(-C'n\tilde{\epsilon}_n^2)$$

For the second term, we note that $\Pi^*(\|\Omega\|_{\infty} \leq B) = \Pi^*\{\max_{1 \leq i \leq q_n} \sum_{j=1}^{q_n} |\omega_{ij}| > B\}$. Now we can have a lower bound in $\Pi^*(\|\Omega\|_{\infty} > B) \geq \Pi^*(\sum_{j=1}^{q_n} |\omega_{ij}| > B)$ for some i. We have already shown that $\Pi^*(\sum_{j=1}^{q_n} |\omega_{ij}| > B) \leq 1 - (1-\eta)^{Q-s_0^{\Omega}} \left[1 - Q-s_0^{\Omega}/B\xi_0\right]^{Q-s_0^{\Omega}}$. Now, for the choice of $B \sim c_2 n\tilde{\epsilon}_n^2$, we have

$$\Pi^*(\|\Omega\|_{\infty} \le B) \le D \exp(-c_2 n\tilde{\epsilon}_n^2)$$

Combining both the inequalities, for a suitable constant $c_3 > 0$,

$$\Pi^*(N \ge r_n + 1) + \Pi^*(\|\Omega\|_{\infty} \le B) \lesssim \exp(-c_3 n\tilde{\epsilon}_n^2)$$

Finally, using Lemma (S.8) in Sagar et al. (2024), for a suitable constant $c_4 > 0$,

$$\Pi(\mathcal{P}_n^c) = \frac{\Pi^*(\mathcal{P}_n^c)}{\Pi(\Omega \in \mathcal{M}_q^+(\lambda))} \lesssim \exp(-c_3 n \tilde{\epsilon}_n^2) \lambda^{-q_n} \exp(C_1 q_n n^{-\frac{1}{2}})$$
$$\lesssim \exp(-c_4 n \tilde{\epsilon}_n^2)$$

This concludes the proof of the lemma.

A.7 Proof of Theorem 7

The proof mirrors the arguments of the proof of Theorem 3 in Wang et al. (2025).

Proof. By definition,

$$\widetilde{b}_{j,k} \neq 0 \iff \frac{|b_{j,k}|}{\omega_{k,k}} > a_n,$$

where $a_n = c \frac{\sqrt{\log p_n}}{\sqrt{n} p_n}$. Hence, to show $S_0 \subseteq \widetilde{S}$ (sure screening), we need to ensure that for each $(j,k) \in S_0$, the above ratio exceeds a_n with high probability.

From standard contraction arguments in Theorem 3, under assumptions (A1)–(A6) we obtain that

$$\max_{j,k} |b_{j,k} - (b_{j,k})_0| \le M\epsilon_n$$

since, we know that $\max_{j,k} |b_{jk}| \leq ||\boldsymbol{B}||_F$. Meanwhile, Theorem 6 shows that whp, Ω is close to Ω_0 in Frobenius norm, and crucially $\omega_{k,k}$ remains bounded away from zero because Ω stays positive-definite. By assumption (A5), Ω_0 has all eigenvalues bounded and away from 0, so for sufficiently large n,

$$\omega_{k,k} \in [\underline{\omega}, \overline{\omega}] \subset (0, \infty)$$
 with high probability.

By assumption (C1), each true nonzero coefficient satisfies

$$|(b_{j,k})_0| \ge \frac{c_3}{n\zeta}$$
 for $(j,k) \in S_0$.

Given the posterior-contraction result in Theorem 3, we pick any small $\delta > 0$. Then for large n, with probability going to 1,

$$|b_{j,k} - (b_{j,k})_0| \le \delta \frac{c_3}{n^{\zeta}}.$$

Hence

$$|b_{j,k}| \geq |(b_{j,k})_0| - \delta \frac{c_3}{n^{\zeta}} \geq (1-\delta) \frac{c_3}{n^{\zeta}}$$
 for large n .

On the other hand, who we also have

 $\omega_{k,k} \leq \overline{\omega}$ for some constant $\overline{\omega} > 0$.

Thus

$$\frac{|b_{j,k}|}{\omega_{k,k}} \geq \frac{(1-\delta) c_3}{\overline{\omega} n^{\zeta}}.$$

Comparing this with the threshold $a_n = c\sqrt{\log p_n}/\sqrt{n}p_n$, note that for $\zeta < 1/4$ and p_n growing sub-exponentially in n, we have

$$n^{-\zeta} \gg \frac{\sqrt{\log p_n}}{\sqrt{n} \, p_n}.$$

Therefore, for sufficiently large n,

$$\frac{|b_{j,k}|}{\omega_{k,k}} > a_n$$
 with high probability.

Consequently, $b_{j,k}$ is not thresholded to zero, i.e. $\tilde{b}_{j,k} \neq 0$ for every $(j,k) \in S_0$. This shows that all truly nonzero entries survive the screening step. In other words,

$$\mathbb{P}(S_0 \subseteq \widetilde{S}) \to 1 \text{ as } n \to \infty.$$

Taking supremum over B_0 just ensures uniformity across all possible true parameter choices. Hence

$$\sup_{\boldsymbol{B}_0} \mathbb{E}_{\boldsymbol{B}_0} \Big[\mathbb{P} \left(S_0 \subseteq \widetilde{S} \mid \boldsymbol{Y}_n \right) \Big] \longrightarrow 1,$$

which completes the proof of the sure-screening property.

B Additional simulation details and results

B.1 Simulating the different covariance structures

Following the settings discussed in Shen et al. (2024), for the AR(1) model, we specifically set $(\Omega^{-1})_{k,k'} = 0.7^{|k-k'|}$ so that $\omega_{k,k'} = 0$ whenever |k-k'| > 1. In the AR(2) model, we set $\omega_{k,k} = 1$, $\omega_{k-1,k} = \omega_{k,k-1} = 0.5$, and $\omega_{k-2,k} = \omega_{k,k-2} = 0.25$. The block model is obtained by partitioning Ω^{-1} into four $q/2 \times q/2$ blocks and setting all entries in the off-diagonal blocks to zero. Then, we take $\sigma_{k,k} = 1$ and $\sigma_{k,k'} = 0.5$ for $1 \le k \ne k' \le q/2$ and for $q/2 + 1 \le k \ne k' \le q$. For the star graph, we choose $\omega_{k,k} = 1$, $\omega_{1,k} = \omega_{k,1} = 0.1$ for each k > 1, and force the remaining off-diagonal elements of Ω equal to zero. The small-world and tree networks necessitate the initial generation of an appropriate random graph and then drawing Ω from a G-Wishart distribution with three degrees of freedom and an identity scale matrix (Roverato, 2002). The Watts-Strogatz model (Watts and Strogatz, 1998) with a single community and rewiring probability of 0.1 was used to generate the small-world graph. Finally, the tree graph was generated by running a loop-erased random walk on a complete graph.

B.2 Additional simulation results

The support recovery performance for Ω in Table B1 under mixed-mSSL shows consistently high specificity across most graph structures, indicating a strong ability to avoid false positives when detecting conditional independencies among responses. In particular, specificity values are generally high across all settings and graph types, except in the Tree Network scenario where it is reported as NaN. This NaN arises because the true precision matrix in the Tree Network is fully dense, i.e., there are no true zero entries in the off-diagonal positions.

Table B2 shows that sepglm finds the largest share of true signals (highest SEN) but at the expense of many false positives, whereas mixed-mSSL keeps the highest SPEC or PREC and nearly the best ACC sacrificing SEN. mt-MBSP displays a similar conservative behavior to mixed-mSSL, and sepSSL sits in between with moderate SEN but low SPEC and PREC. mixed-mSSL still consistently achieves the best predictive accuracy metrics.

Overall, in Table B3, the disjoint-uniform signals make all the methods slightly bolder (higher SEN) compared to Table B2. mixed-mSSL offers a decent balance between finding real effects and controlling false discoveries, while also giving the best out-of-sample predictions.

Table B1: Support-recovery for Ω under mixed-mSSL across six graph structures and three (n, p, q) settings. For each block, we report sensitivity (SEN), specificity (SPEC), precision (PREC) and accuracy (ACC) under two signal regimes: $\mathcal{U}[-5, 5]$ vs. $\mathcal{U}[-5, -2] \cup [2, 5]$.

Scenario		<i>U</i> [-	-5, 5]			$\mathcal{U}[-5,-2]$	$[2] \cup [2, 5]$	
	SEN	SPEC	PREC	ACC	SEN	SPEC	PREC	ACC
		(n,	p,q) = (2	00, 500,	4)			
AR1	0.23	0.81	0.51	0.52	0.26	0.76	0.52	0.51
AR2	0.22	0.77	0.83	0.31	0.25	0.77	0.84	0.33
Block Diagonal	0.25	0.80	0.35	0.62	0.25	0.76	0.33	0.59
Star Graph	0.19	0.75	0.43	0.47	0.20	0.72	0.42	0.46
Small World	0.23	0.80	0.70	0.42	0.25	0.75	0.69	0.42
Tree Network	0.94	NaN	1.00	0.94	0.94	NaN	1.00	0.94
		(n, j)	p,q) = (50	00, 1000	,4)			
AR1	0.52	0.58	0.58	0.55	0.47	0.54	0.50	0.50
AR2	0.48	0.63	0.89	0.51	0.46	0.53	0.83	0.48
Block Diagonal	0.49	0.56	0.40	0.54	0.49	0.55	0.34	0.53
Star Graph	0.43	0.50	0.45	0.46	0.45	0.50	0.46	0.46
Small World	0.49	0.52	0.68	0.50	0.50	0.53	0.68	0.51
Tree Network	0.47	NaN	1.00	0.47	0.47	NaN	1.00	0.47
		(n, j)	p,q) = (80	00, 1000	,6)			
AR1	0.18	0.81	0.34	0.60	0.31	0.66	0.32	0.55
AR2	0.20	0.82	0.66	0.45	0.30	0.66	0.56	0.45
Block Diagonal	0.17	0.81	0.37	0.56	0.30	0.66	0.36	0.52
Star Graph	0.22	0.83	0.40	0.63	0.29	0.67	0.30	0.55
Small World	0.18	0.80	0.40	0.56	0.32	0.68	0.39	0.53
Tree Network	0.36	NaN	1.00	0.36	0.55	NaN	1.00	0.55

Table B2: Support recovery and predictive performance across different covariance structures with (n, p, q) = (500, 1000, 4) under the signal setting $\mathcal{U}[-5, 5]$.

Scenario	Method		Support	recovery	7		Predictive		
Scenario	11201104	SEN	SPEC	PREC	ACC	TIME(s)	$\overline{ ext{RFE}}$	RMSE	AUC
	mt-MBSP	0.20	0.94	0.62	0.72	1239.60	62.05	1.64	0.59
AR1	sepSSL	0.42	0.78	0.46	0.67	2.60	61.66	1.05	0.54
	sepglm	0.55	0.75	0.48	0.69	10.22	61.48	0.49	0.61
	mixed-mSSL	0.16	0.95	0.67	0.71	277.20	61.42	0.48	0.63
	mt-MBSP	0.19	0.95	0.64	0.72	915.60	62.04	1.64	0.59
AR2	sepSSL	0.42	0.78	0.46	0.68	1.60	61.66	1.05	0.55
	sepglm	0.55	0.75	0.48	0.69	5.76	61.48	0.49	0.60
	mixed-mSSL	0.15	0.95	0.67	0.71	375.60	61.42	0.49	0.63
	mt-MBSP	0.20	0.94	0.61	0.72	871.74	62.04	1.64	0.59
Block Diagonal	sepSSL	0.43	0.78	0.46	0.67	1.47	61.67	1.04	0.54
	sepglm	0.55	0.75	0.49	0.69	5.30	61.48	0.49	0.60
	${\tt mixed-mSSL}$	0.16	0.95	0.65	0.71	14.52	61.42	0.48	0.63
	mt-MBSP	0.19	0.94	0.63	0.71	449.40	62.04	1.64	0.59
Star Graph	sepSSL	0.43	0.79	0.46	0.68	1.09	61.66	1.05	0.54
	sepglm	0.54	0.75	0.48	0.69	3.51	61.49	0.49	0.59
	${\tt mixed-mSSL}$	0.16	0.95	0.67	0.71	19.97	61.43	0.48	0.63
	mt-MBSP	0.19	0.95	0.62	0.72	459.00	62.05	1.64	0.60
Small World	sepSSL	0.42	0.78	0.46	0.68	1.15	61.66	1.03	0.54
	sepglm	0.54	0.75	0.49	0.69	3.63	61.48	0.50	0.60
	${\tt mixed-mSSL}$	0.16	0.95	0.65	0.71	24.58	61.43	0.50	0.62
	mt-MBSP	0.19	0.95	0.63	0.72	491.40	62.04	1.64	0.59
Tree Network	sepSSL	0.43	0.78	0.46	0.68	1.23	61.66	1.05	0.54
	sepglm	0.55	0.75	0.48	0.69	3.93	61.48	0.49	0.59
	${\tt mixed-mSSL}$	0.15	0.95	0.68	0.72	26.87	61.42	0.48	0.63

Table B3: Support recovery and predictive performance across different covariance structures with (n, p, q) = (500, 1000, 4) under the signal setting $\mathcal{U}[-5, -2] \cup [2, 5]$.

Scenario	Method		Support	recovery	7		Predictive		
Scenario	Method	SEN	SPEC	PREC	ACC	TIME(s)	$\overline{ ext{RFE}}$	RMSE	AUC
	mt-MBSP	0.19	0.93	0.55	0.71	460.80	77.50	1.64	0.59
AR1	sepSSL	0.43	0.78	0.46	0.67	1.09	77.20	1.08	0.55
	sepglm	0.55	0.75	0.48	0.69	3.64	77.05	0.64	0.60
	mixed-mSSL	0.32	0.86	0.52	0.70	5.84	76.99	0.65	0.63
	mt-MBSP	0.19	0.93	0.56	0.71	442.80	77.49	1.64	0.59
AR2	sepSSL	0.43	0.78	0.46	0.67	1.08	77.20	1.14	0.53
	sepglm	0.55	0.74	0.48	0.68	3.57	77.07	0.66	0.60
	mixed-mSSL	0.33	0.86	0.51	0.71	5.74	76.99	0.65	0.62
	mt-MBSP	0.19	0.93	0.55	0.71	477.60	77.50	1.64	0.59
Block Diagonal	sepSSL	0.43	0.78	0.46	0.67	1.18	77.20	1.06	0.53
	sepglm	0.55	0.75	0.48	0.69	4.00	77.07	0.65	0.60
	mixed-mSSL	0.33	0.86	0.51	0.70	6.12	76.99	0.65	0.62
	mt-MBSP	0.19	0.93	0.56	0.71	510.24	77.50	1.64	0.58
Star Graph	sepSSL	0.43	0.78	0.46	0.67	$\bf 1.29$	77.20	1.08	0.53
	sepglm	0.54	0.75	0.48	0.69	4.35	77.06	0.64	0.60
	${\tt mixed-mSSL}$	0.33	0.86	0.52	0.71	7.27	76.99	0.64	0.62
	mt-MBSP	0.19	0.93	0.54	0.70	475.32	77.50	1.64	0.59
Small World	sepSSL	0.43	0.78	0.46	0.67	$\bf 1.25$	77.20	1.12	0.53
	sepglm	0.54	0.75	0.48	0.69	4.12	77.07	0.65	0.60
	${\tt mixed-mSSL}$	0.32	0.86	0.51	0.70	6.28	76.99	0.65	0.62
	mt-MBSP	0.18	0.93	0.55	0.71	486.30	77.49	1.64	0.59
Tree Network	sepSSL	0.44	0.78	0.46	0.67	1.34	77.20	1.14	0.53
	sepglm	0.55	0.74	0.48	0.68	4.20	77.06	0.64	0.60
	mixed-mSSL	0.33	0.86	0.52	0.70	7.42	76.99	0.65	0.63

Table B4: Support recovery and predictive performance across different covariance structures with (n, p, q) = (800, 1000, 6) under the signal setting $\mathcal{U}[-5, 5]$.

Scenario	Method		Support	recovery	7		F	Predictive)
Scenario	Method	SEN	SPEC	PREC	ACC	TIME(s)	$\overline{ ext{RFE}}$	RMSE	AUC
	mt-MBSP	0.49	0.98	0.92	0.83	4269.60	79.04	1.44	0.60
AR1	sepSSL	0.58	0.72	0.47	0.68	6.76	78.27	0.92	0.59
	sepglm	0.73	0.75	0.56	0.75	33.12	78.06	0.15	0.65
	mixed-mSSL	0.51	0.86	0.60	0.75	442.56	77.97	0.13	0.65
	mt-MBSP	0.49	0.97	0.90	0.83	2127.60	79.04	1.44	0.61
AR2	sepSSL	0.58	0.70	0.45	0.66	4.02	78.27	0.92	0.59
	sepglm	0.73	0.75	0.56	0.74	13.96	78.06	0.15	0.66
	mixed-mSSL	0.50	0.86	0.60	0.75	269.40	77.98	0.14	0.65
	mt-MBSP	0.49	0.98	0.92	0.83	4302.00	79.04	1.44	0.60
Block Diagonal	sepSSL	0.58	0.72	0.47	0.68	6.78	78.27	0.92	0.59
	sepglm	0.73	0.75	0.56	0.74	32.99	78.06	0.15	0.65
	${\tt mixed-mSSL}$	0.50	0.86	0.61	0.75	431.28	77.97	0.13	0.66
	mt-MBSP	0.49	0.98	0.92	0.83	2274.60	79.04	1.44	0.61
Star Graph	sepSSL	0.59	0.72	0.47	0.68	4.19	78.27	0.91	0.59
	sepglm	0.73	0.75	0.56	0.75	15.40	78.06	0.15	0.65
	${\tt mixed-mSSL}$	0.50	0.86	0.61	0.76	271.80	77.97	0.13	0.65
	mt-MBSP	0.47	0.94	0.77	0.80	1419.00	79.04	1.45	0.61
Small World	sepSSL	0.58	0.69	0.45	0.66	2.58	78.27	0.94	0.58
	sepglm	0.73	0.73	0.54	0.73	8.78	78.07	0.17	0.65
	${\tt mixed-mSSL}$	0.49	0.83	0.55	0.73	159.00	77.99	0.18	0.65
	mt-MBSP	0.49	0.98	0.92	0.83	2110.20	79.04	1.44	0.60
Tree Network	sepSSL	0.58	0.71	0.47	0.67	3.90	78.27	0.92	0.59
	sepglm	0.73	0.75	0.56	0.74	13.74	78.06	0.15	0.66
	mixed-mSSL	0.50	0.86	0.61	0.75	227.88	77.97	0.13	0.65

Table B5: Support recovery and predictive performance across different covariance structures with (n, p, q) = (800, 1000, 6) under the signal setting $\mathcal{U}[-5, -2] \cup [2, 5]$.

Scenario	Method		Support	recovery	7		F	Predictive	;
Scenario	Method	SEN	SPEC	PREC	ACC	TIME(s)	$\overline{ ext{RFE}}$	RMSE	AUC
	mt-MBSP	0.53	0.98	0.94	0.85	2127.00	98.91	1.44	0.60
AR1	sepSSL	0.60	0.70	0.46	0.67	4.06	98.23	0.96	0.57
	sepglm	0.78	0.73	0.55	0.74	15.51	97.94	0.17	0.64
	mixed-mSSL	0.51	0.86	0.61	0.76	354.30	97.82	0.13	0.65
	mt-MBSP	0.53	0.98	0.93	0.84	2064.60	98.92	1.44	0.60
AR2	sepSSL	0.60	0.69	0.45	0.66	3.83	98.23	0.96	0.57
	sepglm	0.78	0.72	0.55	0.74	14.25	97.94	0.18	0.65
	mixed-mSSL	0.51	0.86	0.60	0.75	342.66	97.82	0.13	0.65
	mt-MBSP	0.53	0.98	0.94	0.85	2046.60	98.91	1.44	0.60
Block Diagonal	sepSSL	0.60	0.69	0.45	0.66	3.69	98.23	0.96	0.58
	sepglm	0.78	0.73	0.55	0.74	14.47	97.94	0.17	0.65
	${\tt mixed-mSSL}$	0.50	0.86	0.60	0.76	319.20	97.82	0.13	0.64
	mt-MBSP	0.53	0.98	0.94	0.85	1956.60	98.91	1.45	0.59
Star Graph	sepSSL	0.60	0.71	0.47	0.68	3.67	98.23	0.95	0.58
	sepglm	0.78	0.73	0.55	0.74	13.76	97.95	0.19	0.65
	${\tt mixed-mSSL}$	0.51	0.86	0.61	0.76	294.96	97.84	0.17	0.65
	mt-MBSP	0.52	0.93	0.78	0.81	1759.68	98.92	1.44	0.60
Small World	sepSSL	0.60	0.68	0.45	0.66	3.51	98.23	0.95	0.59
	sepglm	0.78	0.71	0.54	0.73	12.45	97.95	0.19	0.64
	mixed-mSSL	0.51	0.83	0.57	0.74	261.60	97.84	0.17	0.65
	mt-MBSP	0.53	0.98	0.94	0.85	1807.74	98.91	1.44	0.60
Tree Network	sepSSL	0.60	0.69	0.46	0.67	3.44	98.23	0.98	0.58
	sepglm	0.78	0.72	0.55	0.74	13.89	97.94	0.17	0.64
	mixed-mSSL	0.51	0.87	0.61	0.76	260.10	97.82	0.12	0.65

The common story for Table B4 and Table B5 is the superior predictive performance for mixed-mSSL and a balanced trade-off between SEN, SPEC and PREC. It is worth noting that in this large n and large p setting, mt-MBSP trades enormous computation for near-perfect PREC and SPEC but middling prediction.

B.3 Hyperparameter Sensitivity Analysis

Below is a sensitivity analysis for the two spike–slab penalty hyperparameters in the AR1 setting with (n, p, q) = (200, 500, 4) under the signal setting $\mathcal{U}[-5, -2] \cup [2, 5]$. We compare the default penalties (λ_0, λ_1) elaborated in Section 3 to halved penalties $(\lambda_0/2, \lambda_1/2)$ and doubled penalties $(2\lambda_0, 2\lambda_1)$. Table B6 shows that halving both spike-penalty parameters $(\lambda_0/2, \lambda_1/2)$ yields higher sensitivity at the expense of specificity and precision, while doubling them $(2\lambda_0, 2\lambda_1)$ produces

the reverse effect—a conservative fit with very high specificity but low sensitivity. Notably, the predictive metrics remain largely stable across this two-fold range of penalties, demonstrating that mixed-mSSL's out-of-sample performance is robust to moderate hyperparameter changes.

Table B6: Hyperparameter sensitivity for mixed-mSSL under AR(1), (n, p, q) = (200, 500, 4).

Penalties		Sup	port		P	redictive	
	SEN	SPEC	PREC	ACC	RFE	RMSE	AUC
$\frac{\left(\frac{\lambda_0}{2}, \frac{\lambda_1}{2}\right)}{\left(\frac{\lambda_0}{2}, \frac{\lambda_1}{2}\right)}$	0.42	0.80	0.47	0.69	54.57	0.78	0.60
(λ_0, λ_1) (default) $(2\lambda_0, 2\lambda_1)$	$0.35 \\ 0.10$	$0.86 \\ 0.99$	$0.51 \\ 0.78$	$0.70 \\ 0.70$	54.57 54.60	$0.77 \\ 0.80$	$0.60 \\ 0.58$

C Additional details for the real data analyses

C.1 Results for the chronic kidney disease (CKD) application

The top ten important biomarkers identified by Ebiaredoh-Mienye et al. (2022), which are treated as the "gold-standard" for our classification metrics were: Albumin (AL), Hemoglobin (HEMO), Packed Cell Volume (PCV), Red Blood Cell Count (RBCC), Serum Creatinine (SC), Blood Glucose Random (BGR), Blood Urea (BU), Sodium (SOD), White Blood Cell Count (WBCC), and Hypertension (HTN). Table C1 summarizes the set of selected biomarkers for our CKD analysis.

Table C1: CKD biomarkers selected by each method

Method	Selected biomarkers
mixed-mSSL	AL, RBCC, HEMO, DM, BGR, PCV, HTN
mt-MBSP	AL, SC, HEMO, DM, SOD
sepSSL	AL, HEMO, DM, PCV, HTN, BP
sepglm	BP, AL, SU, RBC, PCC, BA, BGR, SC, SOD, HEMO,
	PCV, WBCC, RBCC, HTN, DM, APPET

The key to these biomarker abbreviations are listed below:

Table C2: CKD biomarker abbreviations

$\overline{\text{Code}}$	Description
BP	Blood pressure (mm/Hg)
AL	Albumin (qualitative)
SU	Sugar (qualitative)
RBC	Red blood cells (qualitative)
RBCC	Red blood cell count ($\times 10^6/\mu L$)
PCC	Pus cell clumps (qualitative)
BA	Bacteria (qualitative)
BGR	Random blood glucose (mg/dL)
SC	Serum creatinine (mg/dL)
SOD	Sodium (mEq/L)
HEMO	Hemoglobin (g/dL)
PCV	Packed cell volume (%)
WBCC	White blood cell count ($\times 10^3/\mu L$)
HTN	Hypertension status (yes/no)
DM	Diabetes mellitus status (yes/no)
APPET	Appetite (good/poor)